Vibrational Excitation of HDO Molecule by Electron Impact

Mehdi Adrien Ayouz, Alexandre Faure, Ioan F. Schneider, János Zsolt Mezei, Viatcheslav Kokoouline

atoms

MDPI

Article

Vibrational Excitation of HDO Molecule by Electron Impact

Mehdi Adrien Ayouz [1,2,*], Alexandre Faure [3], Ioan F. Schneider [4,5], János Zsolt Mezei [6] and Viatcheslav Kokoouline [7]

[1] SPMS, CentraleSupélec, Université Paris-Saclay, 8-10 rue Joliot-Curie, F-91190 Gif-sur-Yvette, France
[2] LGPM, CentraleSupélec, Université Paris-Saclay, 8-10 rue Joliot-Curie, F-91190 Gif-sur-Yvette, France
[3] Université Grenoble Alpes, CNRS, IPAG, F-38000 Grenoble, France; alexandre.faure@univ-grenoble-alpes.fr
[4] LOMC CNRS-UMR6294, Université du Havre, F-76058 Le Havre, France; schneidi@univ-lehavre.fr
[5] LAC CNRS-UMR9188, Université Paris-Sud, ENS Cachan, Université Paris-Saclay, F-91405 Orsay, France
[6] HUN-REN Institute for Nuclear Research (ATOMKI), 4026 Debrecen, Hungary; mezeijzs@gmail.com
[7] Department of Physics, University of Central Florida, Orlando, FL 32816, USA; slavako@ucf.edu
* Correspondence: mehdi.ayouz@centralesupelec.fr

Abstract: Cross sections and thermally averaged rate coefficients for the vibrational excitation and de-excitation by electron impact on the HDO molecule are computed using a theoretical approach based entirely on first principles. This approach combines scattering matrices obtained from the UK R-matrix codes for various geometries of the target molecule, three-dimensional vibrational states of HDO, and the vibrational frame transformation. The vibrational states of the molecule are evaluated by solving the Schrödinger equation numerically, without relying on the normal-mode approximation, which is known to be inaccurate for water molecules. As a result, couplings and transitions between the vibrational states of HDO are accurately accounted for. From the calculated cross sections, thermally averaged rate coefficients and their analytical fits are provided. Significant differences between the results for HDO and H_2O are observed. Additionally, an uncertainty assessment of the obtained data is performed for potential use in modeling non-local thermodynamic equilibrium (non-LTE) spectra of water in various astrophysical environments.

Keywords: molecular reactive collisions; vibrational excitation; frame transformation; R-matrix theory; comets; space; water isotopologue; HDO

Academic Editor: Kanti M. Aggarwal

Received: 31 January 2025
Revised: 26 March 2025
Accepted: 28 March 2025
Published: 8 April 2025

Citation: Ayouz, M.A.; Faure, A.; Schneider, I.F.; Mezei, J.Z.; Kokoouline, V. Vibrational Excitation of HDO Molecule by Electron Impact. *Atoms* **2025**, *13*, 32. https://doi.org/10.3390/atoms13040032

1. Introduction

Water, H_2O, is ubiquitous in the Universe, in both the gas and solid phases, and it is the third most abundant molecule after H_2 and CO. The singly deuterated form of water, HDO, is much less abundant (by typically two to five orders of magnitude), but it is also detected in a variety of astrophysical environments, including interstellar and circumstellar regions and planetary and cometary atmospheres (see Ref. [1] and references therein). Observing H_2O and HDO in the same source is particularly interesting because the HDO/H_2O ratio is a unique probe of water history and, in (exo)planets, the evolution of their atmospheres. For instance, this ratio was measured in the protoplanetary disk around the sun-like protostar V883 Ori, giving a value comparable to those of protostellar envelopes and comets [2]. Recently, an unexpected increase in the HDO/H_2O ratio was observed in the Venus mesosphere [3].

The presence or likely presence of HDO in high (above room) temperature environments has motivated the construction of extensive line lists for ro-vibrational transitions. The most recent one is called TBD, and it was computed recently as part of the ExoMol project [4]. This new line list replaces the old VTT line list [5] and comprises energies up

to 41,000 cm^{-1} with a recommended highest temperature limit of 3000 K. It is of great interest for the modeling of (exo)planetary and cometary atmospheres [6]. In such environments, however, local thermodynamical equilibrium (LTE) is not fulfilled everywhere and in addition to an accurate line list, collisional rate coefficients are critical to accurately model the ro-vibrational excitation of molecules, see e.g., Ref. [7] for water-rich exoplanetary atmospheres.

In astrophysical media, the dominant collisional partners for the excitation of target molecules (here HDO) are neutral atoms and molecules (e.g., H and H_2 in the ISM, H_2O, CO and CO_2 in comets) and free electrons. Electron collisions are competitive or even dominant in harsh environments, when the electron fraction typically exceeds 10^{-4}. Such high fractional ionization is observed, for instance, in photon-dominated regions (e.g., at the boundary of molecular clouds) and in comets, where free electrons are thermalized by the neutrals, and the kinetic temperature typically varies between 10 and 10^4 K (see e.g., Ref. [8]). Theoretical rate coefficients for the rotational excitation of HDO (in its ground vibrational state) by H_2 and electron collisions are available in the literature for kinetic temperatures in the ranges of 5–300 K [9] and 100–8000 K [10], respectively. Moreover, the low energy scattering resonances in the rotational excitation of HDO by H_2 were recently studied in a joint theoretical and experimental study [11]. However, to the best of our knowledge, there is no such theoretical or experimental study for the (ro)vibrational excitation of HDO.

In 2024, Ayouz et al. [12] computed cross sections for the vibrational excitation of H_2O, including, for the first time, transitions with more than two-quanta excitations as well as inter-mode transitions. Their theoretical approach is based on first principles and employs numerical vibrational wave functions without recourse to the normal-mode approximation. Their calculations were extensively compared to previous theoretical and experimental data, as reviewed in Ref. [13]. In the present work, we extend the theory of Ref. [12] to treat the vibrational excitation of the singly deuterated isotopologue of water, HDO, with a reduced symmetry point group. The 16 lowest vibrational levels of HDO are considered, i.e., up to level $(v_1v_2v_3)$ = (130) lying about 6800 cm^1 above the ground state, and thermally averaged rate coefficients are obtained for kinetic temperatures up to 10,000 K.

The rest of the article is organized in the following way. Section 2 describes the theoretical approach used in the present calculations. The obtained cross sections and the corresponding rate coefficients are displayed and discussed in Section 3. Section 4 concludes the study.

2. Theoretical Approach

The basic formalism employed in our model is presented in detail in Ref. [12]; we only sketch its major ideas in this section.

2.1. HDO Molecule Properties

HDO molecule is an asymmetric isotopologue of H_2O with the symmetry point group reduced from C_{2v} to C_s at equilibrium. Its electronic structure is equivalent to water with a configuration in the ground state of

$$^1A_1 : 1a'^2\, 2a'^2\, 1a''^2\, 3a'^2\, 1a''^2.$$

The HDO molecule can be characterized by three normal modes of vibration, OD stretching ν_1, bending ν_2, and OH stretching ν_3, with respective frequencies ω_1, ω_2, and ω_3 and corresponding dimensionless coordinates q_1, q_2, and q_3. Due to the mass difference $(m_D/m_H \simeq 2)$, the nuclear dynamics of HDO along the O-H and O-D bonds is expected to be asymmetric with a frequency ω_3 much larger than ω_1.

As the first step of the present theoretical approach, normal-mode frequencies and the matrix of transformation between the Cartesian and normal-mode coordinates are needed. Using the quantum chemistry package MOLPRO [14], we performed the Coupled Cluster Singles, Doubles, and Triples (CCSD(T)) calculations with Hartree–Fock orbitals, followed by the optimization procedure in the C_1 symmetry group. The aug-cc-pVQZ basis set was employed on each atom, including the s, p, d, and f orbitals for the hydrogen and deuterium atoms, while an additional orbital g was added for the oxygen atom. We used a mass of 1.008 u for the hydrogen atom and 2.014 u for the deuterium [15]. The total energy of the molecule decreases from −76.06572148, from the Hartree–Fock self-coherent field calculation to −76.35404102 hartree using CCSD, then to −76.3634191 hartree when adding the triples (T) contribution, and finally stabilizes at −76.3635876 hartree with the CCSD(T) method when combined with the optimization procedure.

Table 1 gives the optimized geometry and vibrational frequencies obtained in the present calculation and compares the results with available experimental data for HDO and H_2O. Normal modes of each molecule are displayed in the table with arrows indicating each mode's direction and magnitude of displacements. Note that the OH stretching mode displacement in HDO is much larger than for the OD stretch according to the frequency values ω_3 and ω_1. Moreover, the present ab initio model is different than the one used for H_2O, in our previous studies [12,16]; it reproduces the experimental frequencies more accurately.

Table 1. HDO properties—equilibrium structure and vibrational frequencies of vibrational modes (in eV)—obtained in this study and compared with experimental data from Ref. [17], and to those of H_2O. Normal modes of both molecules are depicted in each first column, where the arrows indicate the direction and magnitude of displacements for each mode. Ab initio models are slightly different in the present study and in Ref. [12].

HDO			**H_2O**		
Mode (v)	**This Study**	**Exp. [17]**	**Mode** (v)	**Calc. [12,16]**	**Exp. [17,18]**
Bending (010) 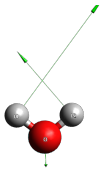	0.179	0.173	Bending (010) 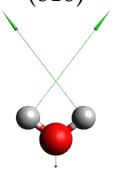	0.207	0.198
OD stretching (100) 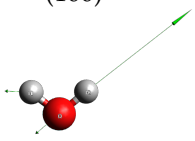	0.349	0.338	Symmetric stretching (100) 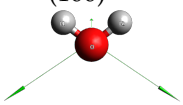	0.472	0.453
OH stretching (001) 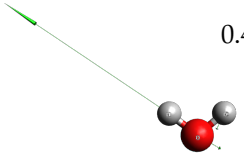	0.482	0.458	Asymmetric stretching (001) 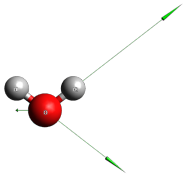	0.488	0.466

Table 1. *Cont.*

HDO			H_2O		
Mode (v)	**This Study**	**Exp. [17]**	**Mode** (v)	**Calc. [12,16]**	**Exp. [17,18]**
Bond lengths $r_1 = r_{OH}$, $r_2 = r_{OD}$ (Å)	0.958	0.956	$r_1 = r_{OH}$, $r_2 = r_{OH}$ (Å)	0.958	0.958
Bond angle $\theta = \widehat{(\vec{r}_1, \vec{r}_2)}$ (Degrees)	104.36	105.20	$\theta = \widehat{(\vec{r}_1, \vec{r}_2)}$ (Degrees)	104.44	104.50

2.2. Fixed Nuclei Scattering Matrix

In the electron-molecule scattering, four fixed geometries $\{\mathbf{q}_1, \mathbf{q}_2, \mathbf{q}_3, \mathbf{q}_4\}$ of the molecule were used. The geometries and the corresponding eigenphase sums are shown in Figure 1. The reactance matrix $\underline{K}(\mathbf{q})$ (K-matrix) was obtained numerically for these geometries using the UK R-matrix codes [19,20] and the Quantemol-N interface [15]. Considering energies below the excitation of the first excited electronic state of the molecule (about 8.3 eV above the ground electronic state at the equilibrium geometry $\mathbf{q}_0 = (0, 0, 0)$), the obtained K-matrices, for each geometry configuration and the scattering electron energy E_{el}, are labeled only by channels (indexes) corresponding to the electronic angular momentum l and its projection λ on the axis perpendicular to the molecular plane.

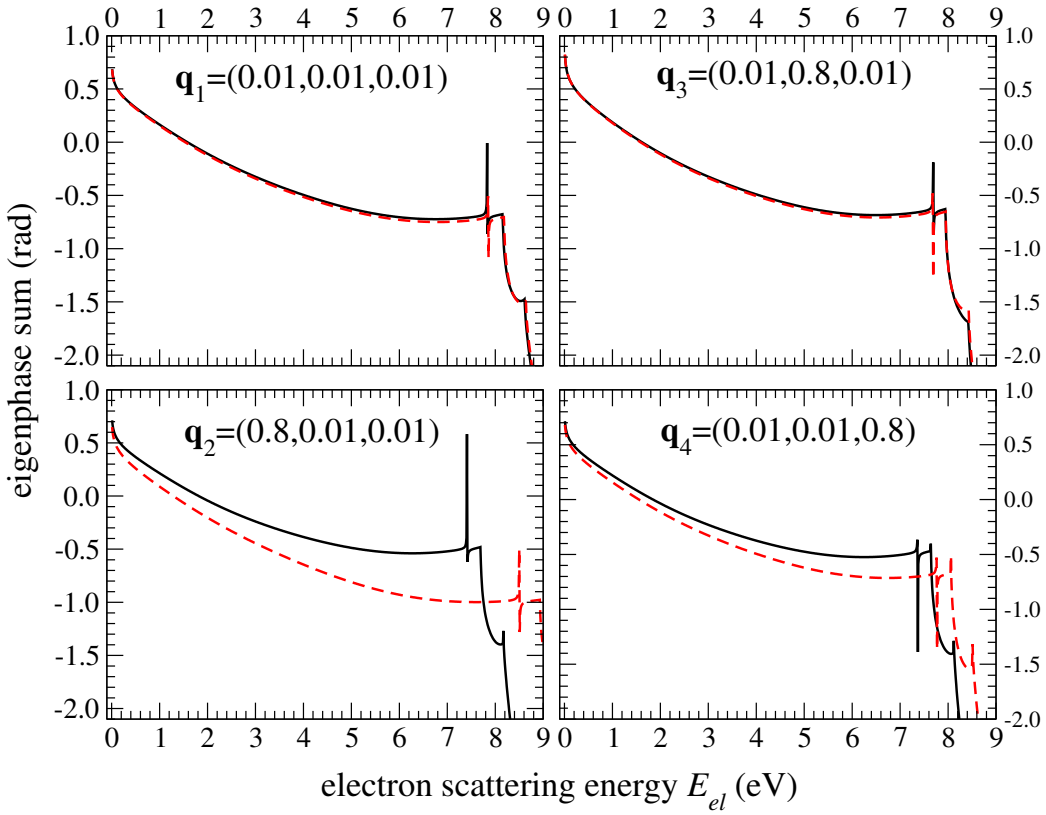

Figure 1. Eigenphase sum as a function of the electron scattering energy E_{el} for different geometry configurations $\mathbf{q}_i = (q_1, q_2, q_3)$ $(i = 1, 2, 3, 4)$ of the HDO molecule (solid black lines) employed for the scattering calculations. For comparison, eigenphase sum for the same geometries are depicted for H_2O (dashed red lines).

Similar to our previous study, devoted to the H_2O molecule [12], we used in the R-matrix calculations the C_1 point group with HDO being in its ground electronic state. The two $1a^2$ core electrons were frozen, and eight electrons were distributed in the active space, including $2-9a$ orbitals. For these calculations, we employed the configuration interaction method (CI) with the cc-pVTZ basis set and the radius of the sphere of the R-matrix of 10 bohr and a partial-wave expansion with continuum Gaussian-type orbitals with $l \leq 4$. This set of calculations, including the cc-pVTZ basis set and the described complete active space (CAS_1), will be referred to hereafter as Model 1. The other models will be introduced further to assess the uncertainty of the obtained results.

Figure 1 shows the eigenphase sum in e^-−HDO scattering (solid line) for the four geometries as a function of the electron energy E_{el}. Dashed lines in the figure indicate eigenphase sums in e^-−H_2O scattering for the same geometries. The electronic structure of H_2O and HDO is identical. Therefore, the equilibrium geometry is the same, and the frequencies of the bending mode of both molecules are similar (see Table 1). The eigenphase sums are the same for the equilibrium geometry and similar for small displacements along the bending coordinates q_2. In the case of the stretching modes ν_1 and ν_3, the significant difference in harmonic frequencies and normal coordinates affects the positions of resonances in the eigenphase sums. Variation in the eigenphase sums is smooth for energies below 7 eV. Thus, the scattering matrix $\underline{S}(\mathbf{q})$ can be employed for the vibrational frame transformation at low scattering energies.

The reactance matrices $\underline{K}(\mathbf{q})$ are transformed into scattering matrices $\underline{S}(\mathbf{q}) = (1 + i\underline{K}(\mathbf{q}))(1 - i\underline{K}(\mathbf{q}))^{-1}$, which are then used to perform the vibrational frame transformation discussed below.

2.3. HDO Vibrational Dynamics

To construct elements of the scattering matrix for transitions from one vibrational level $(v_1v_2v_3) \equiv \boldsymbol{v}$ to another $(v_1'v_2'v_3') \equiv \boldsymbol{v}'$, the vibrational wave functions are needed. For this purpose, the Schrödinger equation for vibrational motion along $\mathbf{q} = (q_1, q_2, q_3)$,

$$\left[-\sum_{i=1}^{3}\frac{\hbar\omega_i}{2}\frac{\partial^2}{\partial q_i^2} + V(\mathbf{q})\right]\psi_v(\mathbf{q}) = \epsilon_v\psi_v(\mathbf{q})\,, \tag{1}$$

is solved numerically [21]. In the above equation, $V(\mathbf{q})$ is the potential energy surface (PES) of H_2O given by Ref. [22]. The PES is obtained in ab initio calculations and refined using empirical rovibrational energy levels. It is given in terms of bond coordinates (r_1, r_2, θ), see Table 1, and then converted to the normal coordinates $\mathbf{q}$ using the transformation matrix and the frequencies.

Since the nuclear dynamics of HDO along the O-H and O-D bonds is asymmetric due to the mass difference $(m_D/m_H \simeq 2)$, a large grid of $18 \times 18 \times 18$ points was used in solving Equation (1) with q_1, q_2, and q_3 varying from -5 to 5 (dimensionless). For these normal mode coordinate intervals, the bound coordinates (r_1, r_2, θ) of HDO vary in the following way: From 0.76 Å to 1.62 Å for r_1, from 0.64 Å to 1.41 Å for r_2, and from 66.80° to 166.51° for θ.

Table 2 gives the obtained energies (in cm^{-1}) of the lowest vibrational levels of HDO and compares them with the experimental data by Tennyson et al. [23] and previous calculations by Zobov et al. [24]. The overall difference in energies of the present results and the experiment for HDO is less than 1%.

In order to perform the frame transformation procedure below and compute the cross sections further, the assignment, $\boldsymbol{v} = (v_1v_2v_3)$, of the low-lying vibrational levels of Table 2 are provided according to the largest square of projection $|\langle v_1, v_2, v_3|\psi_v\rangle|^2$ of the wave function $\psi_v(\mathbf{q})$, obtained numerically, on analytical normal mode states $|v_1, v_2, v_3\rangle$

(harmonic oscillator). Table 3 lists as a matrix the values of $|\langle v_1, v_2, v_3|\psi_v\rangle|^2$ greater than 10^{-1}, i.e., ≥10%. The first row gives the assigned vibrational levels, while the first column stands for the analytical normal modes in the harmonic approximation, classified according to their energies as $\sum_{i=1}^{3} \hbar\omega_i\left(v_i + \frac{1}{2}\right)$. The color scheme is used in the table: The green color denotes the largest element for which the assignment is performed, while the orange color represents the second largest value of $|\langle v_1, v_2, v_3|\psi_v\rangle|^2$.

Table 3 shows that the wave functions of certain vibrational levels have a mixed character. For example, the wave functions of vibrational levels (110) and (030) seem somewhat similar due to the close coincidence between the ω_1 and $2\omega_2$ harmonic frequencies giving almost the same energy for both levels. This result can be confirmed by analyzing the wave functions displayed in Figures 2–4. As depicted in the first two rows of Figure 3, the wave functions of levels (110) and (030) are indeed similar. Analogously, the wave functions of levels (120) and (040) or (101) and (021) are similar to each other, yielding to large values of $|\langle v_1, v_2, v_3|\psi_v\rangle|^2$, as stated in orange in the table. This behavior of the wave functions could be attributed to the anharmonicity of the H_2O PES [22] employed in this study.

Table 2. Energies (in cm^{-1}) of the lowest vibrational levels of HDO, obtained using the PES by Mizus et al. [22], compared with experimental data [23] and previous calculations [24]. The experimental energies are provided in cm^{-1} and in eV (in parentheses). Energies of the H_2O vibrational states are also provided for comparison.

	HDO				H_2O	
(*v*)	**This Work**	**Calc. [24]**	**Exp. [23]**	**Rel. Deviation (%)**	**Calc. [12]**	**Exp. [25]**
(000)	0	0	0	-	0	0
(010)	1394.4249	1403.50	1403.4837 (0.1740)	0.65	1582.1016	1594.7463
(100)	2720.0465	2723.71	2723.6797 (0.3376)	0.13	3656.7438	3657.0533
(020)	2764.8648	2782.02	2782.0111 (0.3449)	0.62	3124.3086	3151.6298
(001)	3700.3818	3707.47	3707.4667 (0.4596)	0.19	3742.8112	3755.9285
(110)	4078.2012	4099.98	4099.9559 (0.5083)	0.53	5223.0359	5234.9756
(030)	4123.3998	4145.48	4145.4731 (0.5139)	0.53	4638.2210	4666.7905
(011)	5061.2551	5089.55	5089.5398 (0.6310)	0.56	5281.1118	5331.2673
(200)	5357.8041	5363.84	5363.8244 (0.6650)	0.11	7195.4949	7201.5399
(040)	5385.3203	5420.00	5420.0414 (0.6719)	0.64	6015.0987	6134.0150
(120)	5474.3136	-	5506.1868 (0.6826)	0.58	6744.5580	6775.0935
(101)	6387.2463	6415.48	6415.4606 (0.7954)	0.44	7239.0123	7249.8169
(021)	6420.4831	6451.91	6451.8998 (0.7999)	0.49	6781.2869	6871.5202
(050)	6645.5504	6690.42	6690.4132 (0.8295)	0.67	7642.5333	7542.3725
(210)	6721.3248	6746.92	6746.9082 (0.8365)	0.38	8737.1399	8761.5816
(130)	6805.1825	-	6849 (0.8491)	0.64	8253.4218	8273.9757

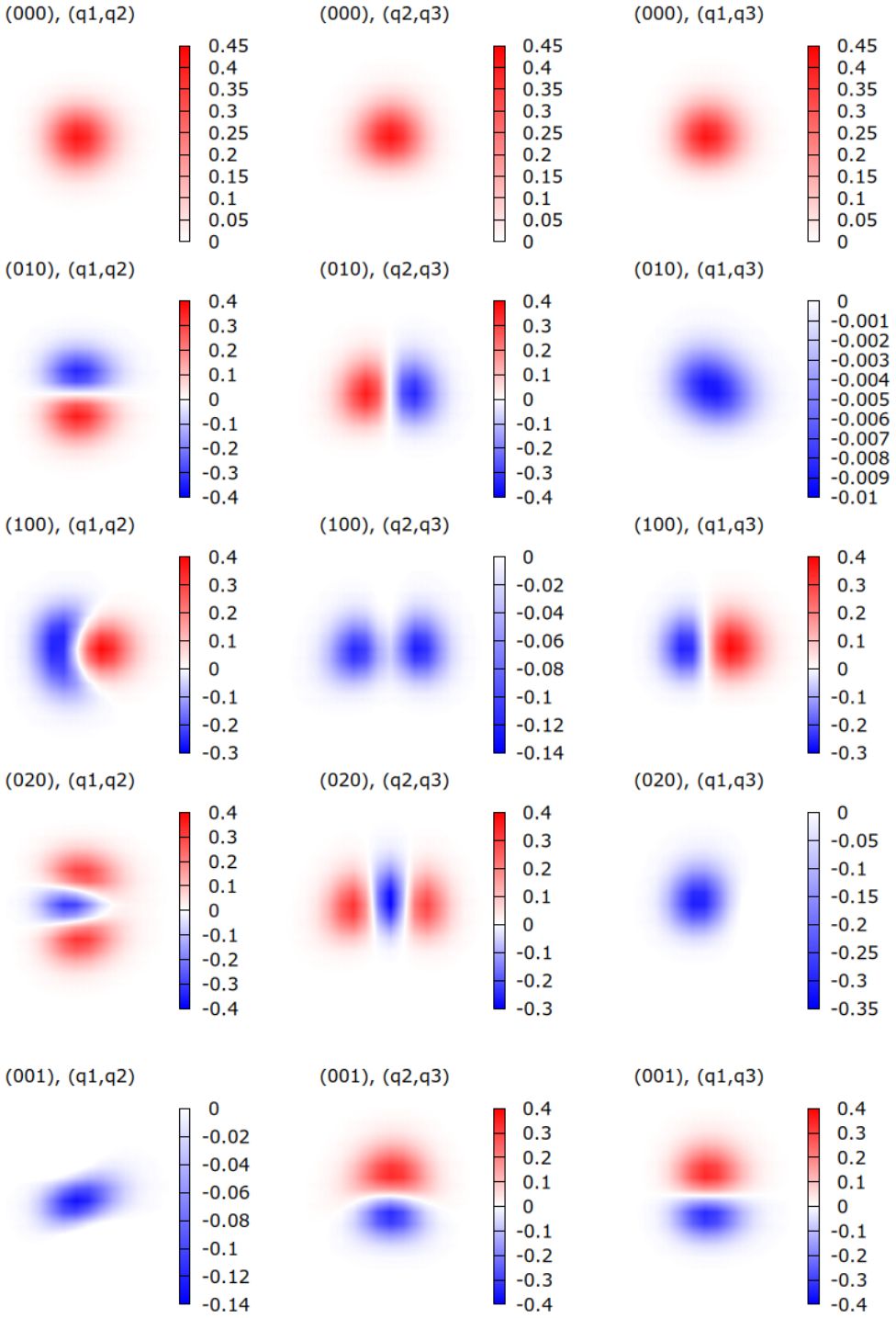

Figure 2. Wave functions of vibrational states of HDO with energies < 7000 cm^{-1} of HDO, shown as intensity plots depending on two coordinates (indicated on the top of each plot), while the third coordinate is fixed at the equilibrium $q_i = 0$.

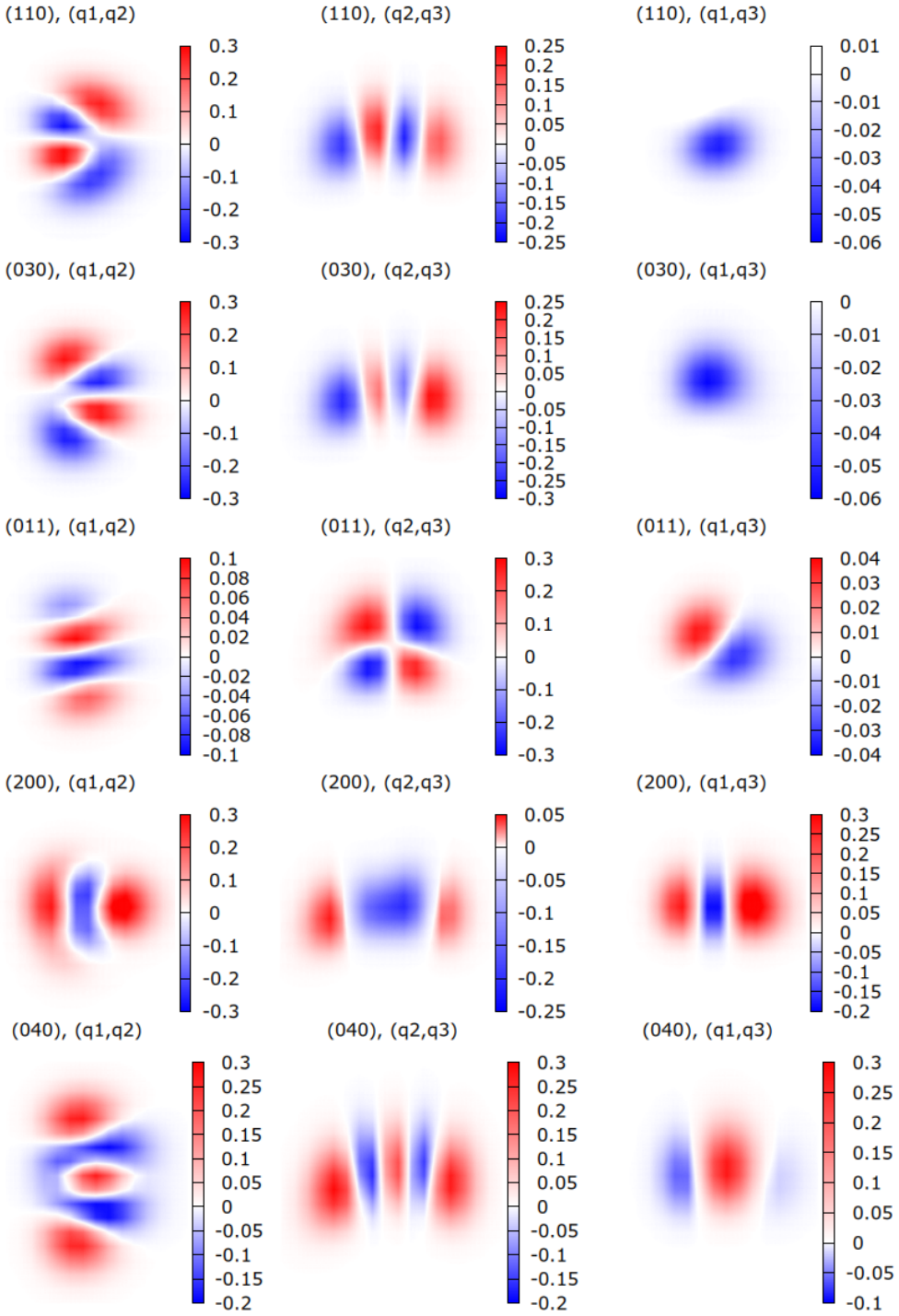

Figure 3. Similar to Figure 2 for several other wave functions.

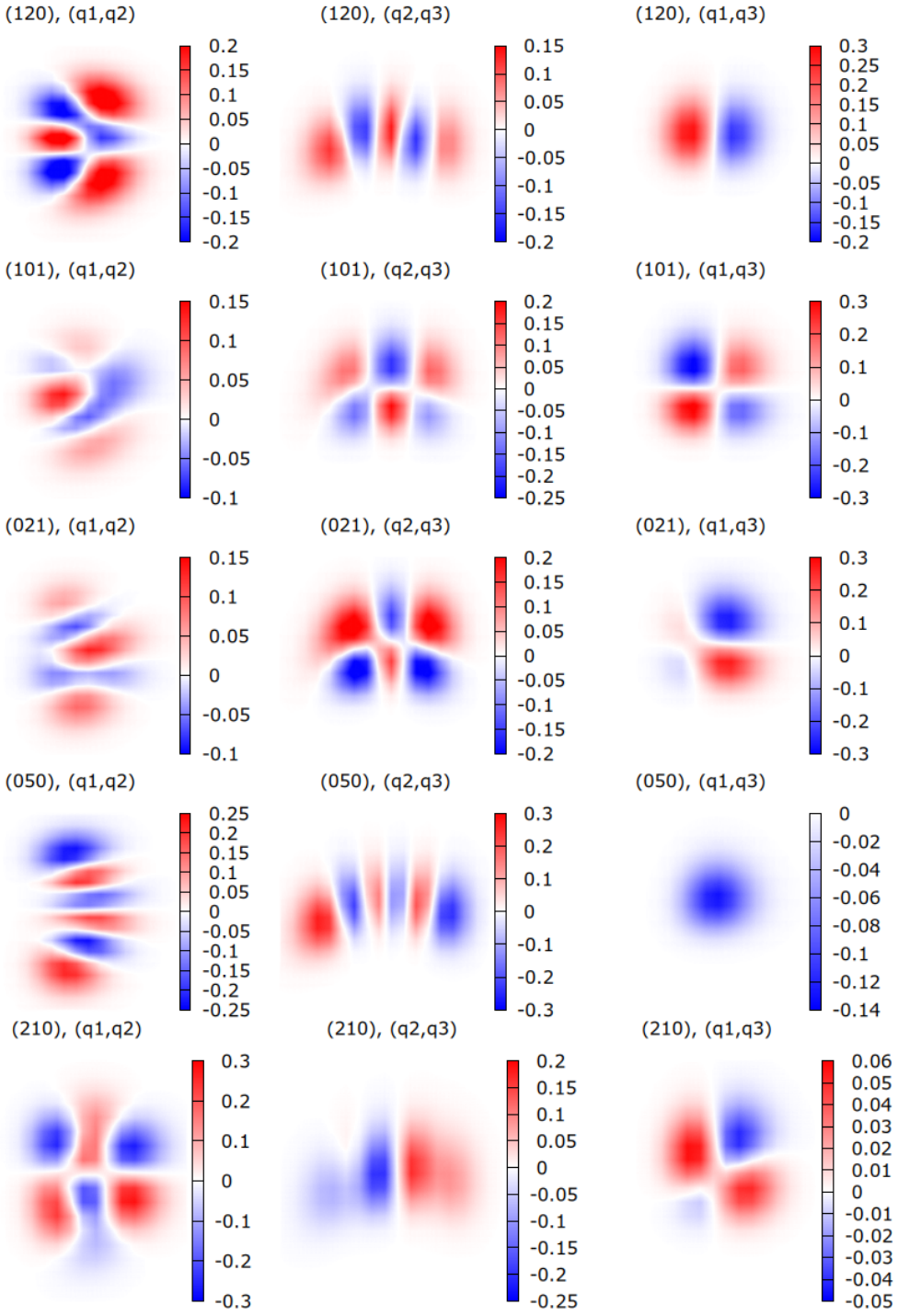

Figure 4. Similar to Figure 2 for several other wave functions.

Table 3. Assignment (v) of the lowest few vibrational levels. The levels, given in Table 1, are assigned according to the largest square of projection $|\langle v_1, v_2, v_3|\psi_v\rangle|^2$ of the wave function ψ_v on the analytical normal-mode states $|v_1, v_2, v_3\rangle$. The green color denotes the largest element for which the assignment is performed, while the orange color represents the second largest value. Curved arrows give the reading direction for each vibrational level assignment.

v_1, v_2, v_3 \ (v)	$\|\psi_{000}\rangle$	$\|\psi_{010}\rangle$	$\|\psi_{100}\rangle$	$\|\psi_{020}\rangle$	$\|\psi_{001}\rangle$	$\|\psi_{110}\rangle$	$\|\psi_{030}\rangle$	$\|\psi_{011}\rangle$	$\|\psi_{200}\rangle$	$\|\psi_{040}\rangle$	$\|\psi_{120}\rangle$	$\|\psi_{101}\rangle$	$\|\psi_{021}\rangle$	$\|\psi_{050}\rangle$	$\|\psi_{210}\rangle$	$\|\psi_{130}\rangle$
$\langle 0,0,0\|$	0.9808															
$\langle 0,1,0\|$		0.9836														
$\langle 1,0,0\|$			0.8371													
$\langle 0,2,0\|$				0.8863												
$\langle 0,0,1\|$					0.8766											
$\langle 1,1,0\|$						0.5002	0.4069									
$\langle 0,3,0\|$						0.3975	0.4957									
$\langle 0,1,1\|$								0.8812								
$\langle 2,0,0\|$									0.6473							
$\langle 1,2,0\|$										0.1440	0.7166					
$\langle 0,4,0\|$										0.6090	0.1445			0.1075		
$\langle 1,0,1\|$												0.5734	0.2148			
$\langle 0,2,1\|$												0.2306	0.6201			
$\langle 2,1,0\|$															0.6247	
$\langle 1,3,0\|$														0.1087		0.6885
$\langle 0,5,0\|$														0.4908		

2.4. The Scattering Matrix for an Electron Colliding with HDO

Using the vibrational wave functions and geometry-fixed S-matrix depending on the normal coordinates, the scattering matrix describing the process

$$e^-(l\lambda) + \mathrm{HDO}(v) \rightarrow e^-(l'\lambda') + \mathrm{HDO}(v'), \tag{2}$$

can be computed using

$$\mathcal{S}^{ex}_{l'\lambda' v', l\lambda v} = \left\langle \psi_{v'}(\mathbf{q}) \middle| S^{ex}_{l'\lambda', l\lambda}(\mathbf{q}) \middle| \psi_v(\mathbf{q}) \right\rangle, \tag{3}$$

where the above bra−kets imply an integration over the three normal coordinates $\mathbf{q} = (q_1, q_2, q_3)$. This integral is evaluated on DVR grid points with the geometry-fixed scattering matrix $S^{ex}_{l'\lambda', l\lambda}(\mathbf{q})$ obtained for each scattering energy E_{el}, using a methodology summarized in Table 4. This methodology includes seven steps in calculations, starting from the R-matrix calculations of the reactance matrix $\underline{K}(\mathbf{q})$—performed on a few geometries (see Figure 1)—followed by the interpolation and extrapolation of the scattering matrix. These latter steps are performed on the scattering phaseshifts $\underline{\Delta}(\mathbf{q})$ instead of $\underline{S}(\mathbf{q})$ due to its smooth behavior with respect to the normal coordinates $\mathbf{q}$.

Table 4. Summary of the methodology for obtaining the scattering matrix $\underline{S}^{ex}(\mathbf{q})$ of Equation (3). The procedure is performed for each scattering energy E_{el} and partial wave $(l'\lambda', l\lambda)$.

Step	Input	Description	Output
(1)	Geometries $\mathbf{q}$ of Figure 1	Calculate the reactance matrix	$\underline{K}(\mathbf{q})$
(2)	$\underline{K}(\mathbf{q})$	Diagonalize $\underline{K}(\mathbf{q})$	Eigenvalues $k(\mathbf{q}) = \tan(\delta(\mathbf{q}))$ and the eigenvectors matrix $\underline{U}$
(3)	$\underline{\delta}(\mathbf{q})$, diagonal matrix of $\delta(\mathbf{q})$	Build the matrix of scattering phaseshifts	$\underline{\Delta}(\mathbf{q}) = \underline{U}\,\underline{\delta}(\mathbf{q})\,\underline{U}^{-1}$
(4)	Elements of $\underline{\Delta}(\mathbf{q})$	Linear fit of $\Delta_{l'\lambda', l\lambda}(\mathbf{q})$ using $\Delta^{fit}_{l'\lambda', l\lambda}(\mathbf{q}) = c_0 + c_1 q_1 + c_2 q_2 + c_3 q_3$	c_0, c_1, c_2 and c_3 for each partial wave $(l'\lambda', l\lambda)$
(5)	$\Delta^{fit}_{l'\lambda', l\lambda}(\mathbf{q})$	Extrapolate $\Delta_{l'\lambda', l\lambda}(\mathbf{q})$	$\Delta^{ex}_{l'\lambda', l\lambda}(\mathbf{q}) = c_0 + c_1 q_1 + c_2 q_2 + c_3 q_3$
(6)	$\underline{\Delta}^{ex}(\mathbf{q})$	Diagonalize $\underline{\Delta}^{ex}(\mathbf{q})$	Eigen phaseshifts $\delta^{ex}(\mathbf{q})$ and eigenvectors matrix $\underline{U}^{ex}$
(7)	Diagonal matrix $\underline{\delta}^{ex}(\mathbf{q})$ from $\delta^{ex}(\mathbf{q})$	Build $\underline{S}^{ex}(\mathbf{q})$	$\underline{S}^{ex}(\mathbf{q}) = \underline{U}^{ex} \exp[2i\underline{\delta}^{ex}(\mathbf{q})](\underline{U}^{ex})^{-1}$

3. Results and Discussions

3.1. Cross Sections

Using the above scattering matrix, the cross section for the $v' \leftarrow v$ process is written as

$$\sigma_{v' \leftarrow v}(E_{el}) = \frac{\pi\hbar^2}{2mE_{el}} \sum_{l'\lambda' l\lambda} \left| S^{ex}_{l'\lambda' v', l\lambda v} - \delta_{v',v}\delta_{l'\lambda', l\lambda} \right|^2, \tag{4}$$

where m and E_{el} are the mass of the electron and the scattering energy.

Figures 5 and 6 show cross sections for the initial levels (000), (010), (100) and (001), in solid lines. The cross sections of e^-−H_2O, published in Ref. [12], are also shown in dashed lines. One can see that the largest cross sections are those for one-quantum (de-)excitation; however, inter-mode transitions are also significant. A comparison to available experimental data and previous calculations of H_2O [16] is given in Figure 7. The cross sections of the HDO isotopologue are in general comparable to those of H_2O, but differences larger than a factor of 3 are also observed, even for large cross sections such as $(010) \leftarrow (100)$ or $(000) \leftarrow (001)$. In addition, some excitation transitions in HDO are (de-)excitation transitions in H_2O due to the different level ordering (e.g., $(020) \leftarrow (100)$). As a result, the D substitution has a significant effect on the vibrational excitation of H_2O, and the cross sections for H_2O cannot be used reliably for HDO, especially at low electron energy. We note that a similar conclusion was drawn for the rotational excitation of HDO by H_2, see Ref. [9].

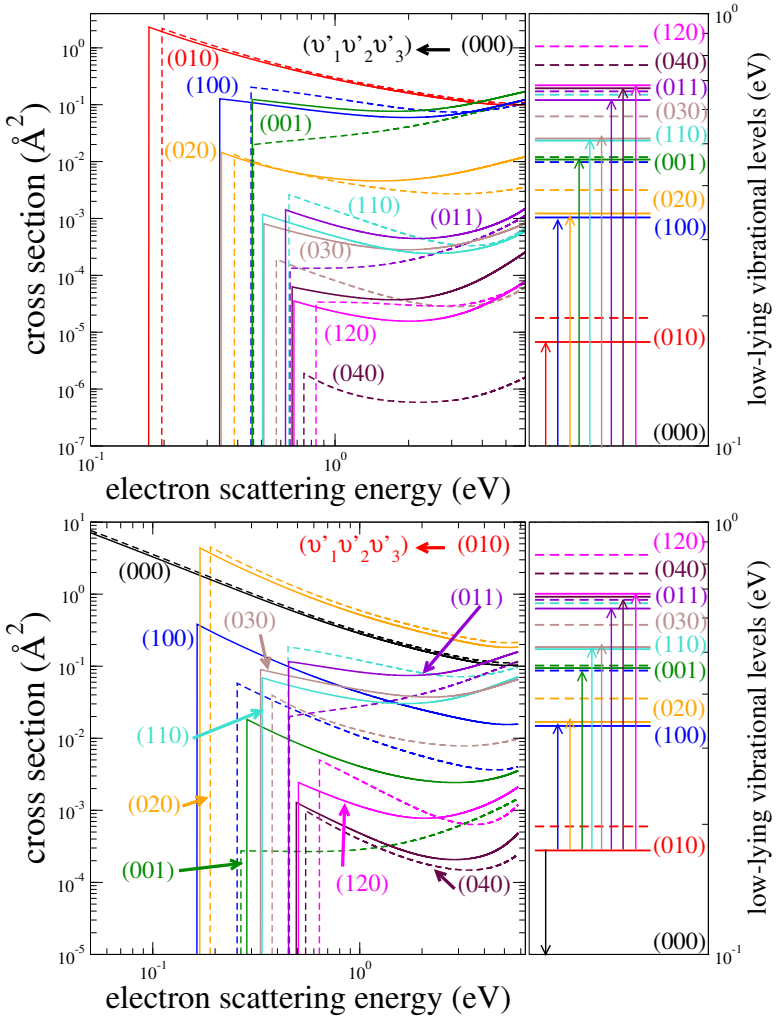

Figure 5. Cross sections of vibrational (de-)excitation of HDO (solid lines) and H_2O (dashed lines) from the vibrational level (000) (the upper panels) or (010) (the lower panels) to several other levels $(v_1'v_2'v_3')$. The corresponding vibrational levels are depicted on the right panels with the same color code. Note that the level (200) is not displayed for clarity reasons.

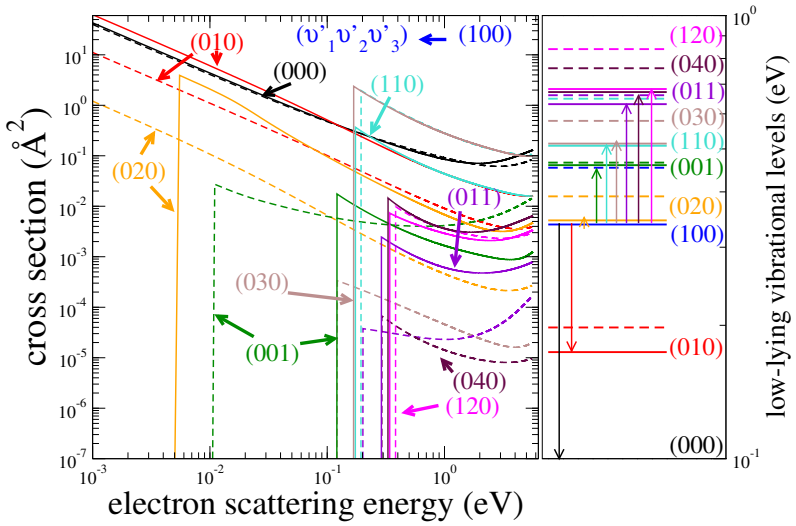

Figure 6. *Cont.*

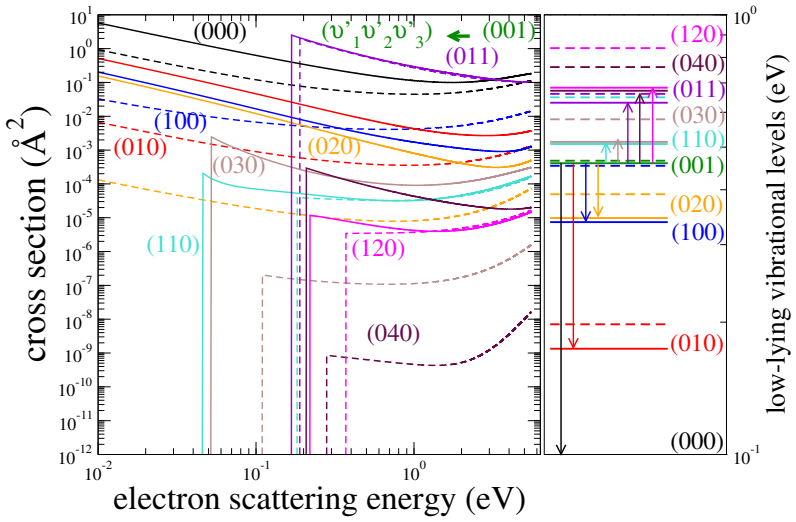

Figure 6. Cross sections of vibrational (de-)excitation of HDO (solid lines) and H_2O (dashed lines) from the vibrational level (100) (the upper panels) or (001) (the lower panels) to several other levels $(v'_1v'_2v'_3)$. The corresponding vibrational levels are depicted on the right panel with the same color code. Note that the level (200) is not displayed for clarity.

The earlier calculations [16] of excitation cross section in H_2O calculations were performed using the normal-mode approximation representing the vibrational motion of the molecule. The normal-mode approximation for H_2O is not particularly accurate. For example, the projection squared of the accurate state (100) having one quantum in the symmetric stretching mode on the normal-mode wave function is only about 83%, while for the state (200), it is only 47%. Therefore, the uncertainty in the cross section calculations performed with the normal mode approximation is, at best, 20% for the $(000) - (100)$ transition and 50% for the $(000) - (200)$ transition. In the 2024 study [12], the vibrational wave functions were obtained solving the 3-dimensional vibrational Schrodinger equation numerically, i.e., the vibrational wave functions were much more accurate. Otherwise, the theoretical methods were the same in the two studies. Therefore, the results obtained in [12] are a priori more accurate. The cross section obtained in the 2024 study is lower than the experiment, especially for excitation of the stretching mode. The reason for the disagreement is not clear. One possibility is that it could be due to the rotational coupling, which is neglected in the theoretical approach.

Calculations for HDO were performed using accurate vibrational wave functions with the same method as it was used in the 2024 study of H_2O. No experimental data exist on vibrational excitation of HDO. Assuming that the experimental data for H_2O (not the theory) should be taken as a benchmark, and given that the theory agrees with the experiment for excitation of the bending mode, one can conclude that the theoretical cross section for the excitation of the bending mode in HDO is accurate, while the theoretical results for the stretching modes could be underestimated by a factor of 2–4.

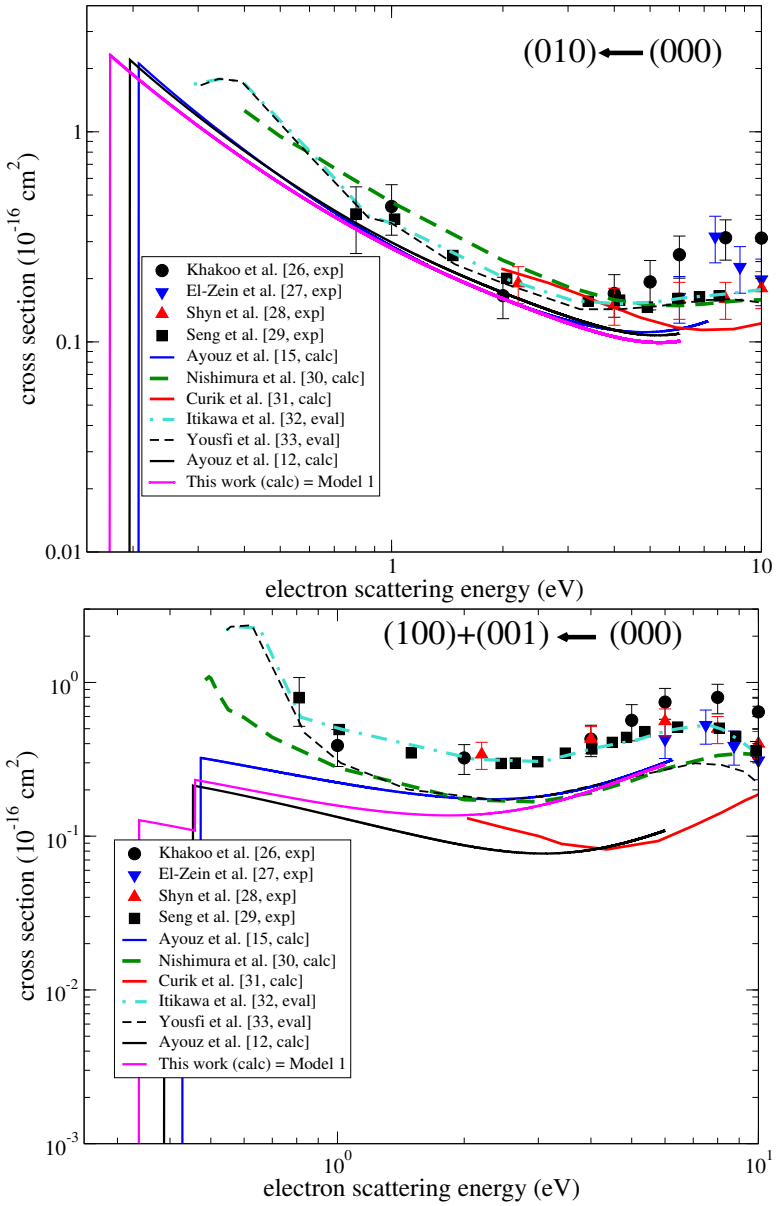

Figure 7. Comparison of cross sections available in the literature [26–33] for the excitation of the bending $(010) \leftarrow (000)$ (top panels) and stretching $(100) + (001) \leftarrow (000)$ (low panels) modes of H_2O. The pink solid line is the theoretical result obtained in this work for HDO, while the black and blue lines are for H_2O from previous studies [12,16].

3.2. Rate Coefficients

The thermally averaged rate coefficient $\alpha_{v' \leftarrow v}(T)$ is obtained as

$$\alpha_{v' \leftarrow v}(T) = \sqrt{\frac{8}{\pi m (k_b T)^3}} \int_0^\infty \sigma_{v' \leftarrow v}(E_{el}) \exp\left(-\frac{E_{el}}{k_b T}\right) E_{el} dE_{el}\,, \tag{5}$$

where k_b and T are the Boltzmann coefficient and the temperature, respectively. Figures 8 and 9 show examples of rate coefficients for initial levels (000), (010), (100), and (001). As for the cross sections, the largest rate coefficients are those for one-quantum (de-)excitations, and their differences with the H_2O coefficients exceed a factor of 3 for some transitions.

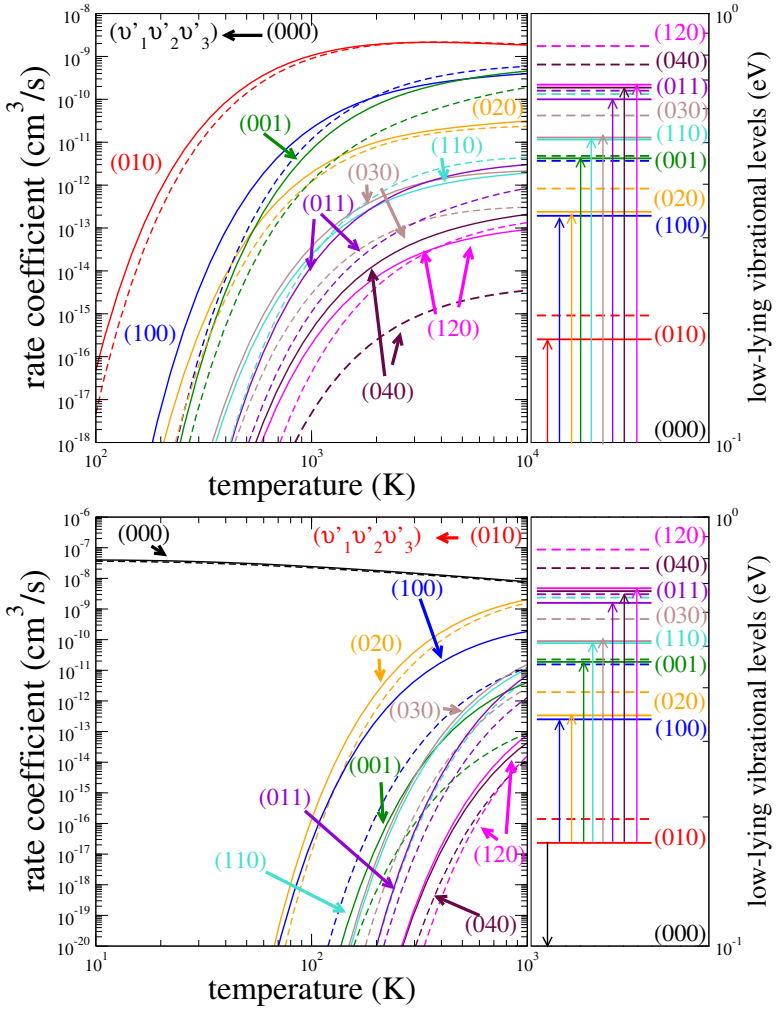

Figure 8. Rate coefficients for the excitation of vibrational (de-)excitation of HDO (solid lines) and H_2O (dashed lines) from the vibrational level (000) (the upper panels) or (010) (the lower panels) to several other levels $(v_1'v_2'v_3')$. The corresponding vibrational levels are depicted on the right panel with the same color code. Note that the level (200) is not displayed for clarity. The color code is the same as in Figure 5.

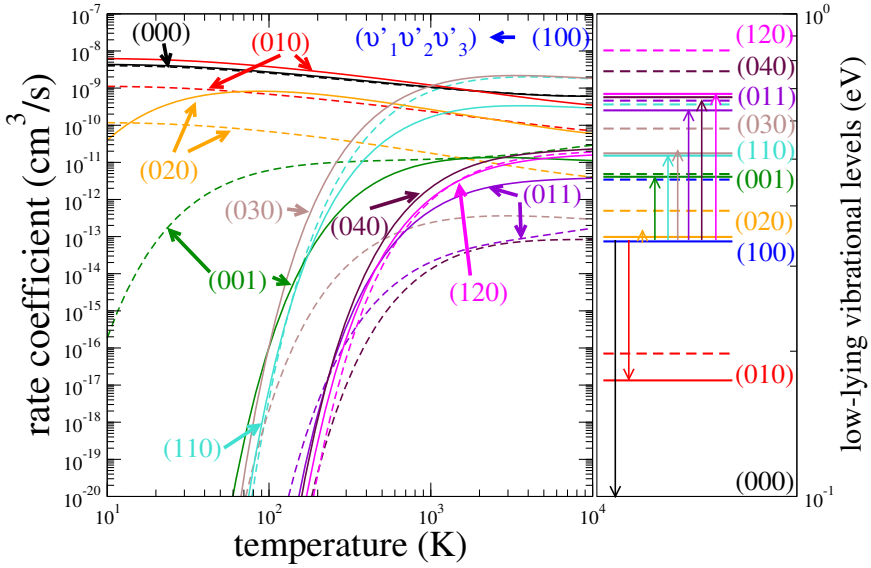

Figure 9. *Cont.*

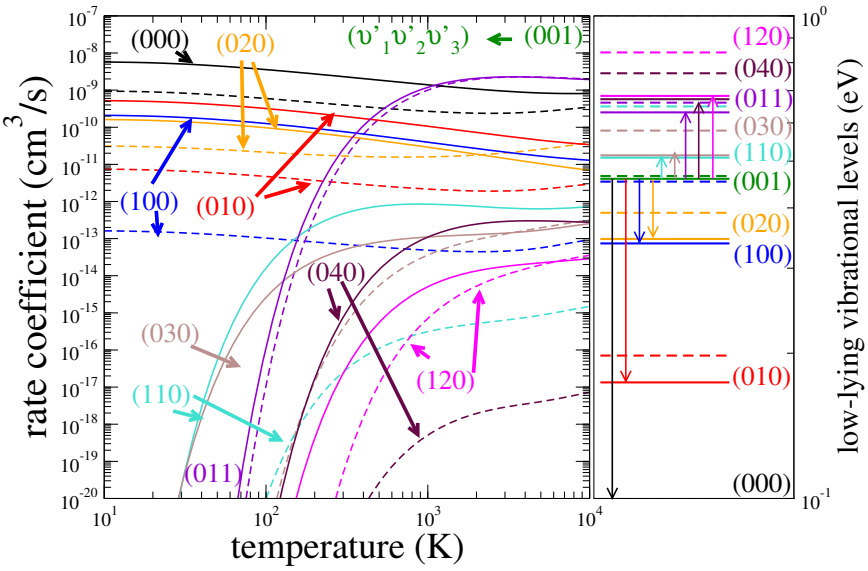

Figure 9. Rate coefficients for the excitation of vibrational (de-)excitation of HDO (solid lines) and H_2O (dashed lines) from the vibrational level (100) (the upper panel) or (001) (the lower panel) to several other levels $(v'_1v'_2v'_3)$. The corresponding vibrational levels are depicted on the right panel with the same color code. Note that the level (200) is not displayed for clarity. The color code is the same as in Figure 6.

Similar to previous studies [12,34] and for simplicity of use, we fitted the obtained rate coefficients to an analytical formula

$$\alpha^{fit}_{v'\leftarrow v}(T) = \frac{1}{\sqrt{T}} \exp\left(-\frac{\Delta_{v',v}}{T}\right) 10^{P(v'\leftarrow v)}, \tag{6}$$

where

$$P(\boldsymbol{v}' \leftarrow \boldsymbol{v}) = a_0 + a_1 x + a_2 x^2 + a_3 x^3, \tag{7}$$

and the coefficients a_i $(i = 0, 1, 2, 3)$ are fitting parameters. The quantity $10^{P(v'\leftarrow v)}$ is roughly the (de-)excitation probability for transition $\boldsymbol{v}' \leftarrow \boldsymbol{v}$ and $P(\boldsymbol{v}' \leftarrow \boldsymbol{v})$ is a smooth function of temperature. Figure 10 shows $P(\boldsymbol{v}' \leftarrow \boldsymbol{v})$ for a few transitions from the ground level $\boldsymbol{v} = (000)$ to several final $\boldsymbol{v}'$ vibrational levels as a function of $x = \log_{10}(T/300\text{K})$. In the above Equation (6), $\Delta_{v',v}$ represents the threshold energy for the transition

$$\Delta_{v',v} = \begin{cases} E_{v'} - E_v > 0 & \text{for excitation,} \\ 0 & \text{for de-excitation.} \end{cases} \tag{8}$$

To employ Formula (6) with fitted parameters a_i given in Appendix A Tables A1–A6 for each pair of transitions $(v'_1v'_2v'_3) \leftrightarrow (v_1v_2v_3)$, the temperature T should be in kelvins. For instance, at $T = 300$ K, the (de-)excitation probability reads as 10^{a_0}, because $x = 0$ for $T = 300$ K (vertical dashed line in Figure 10).

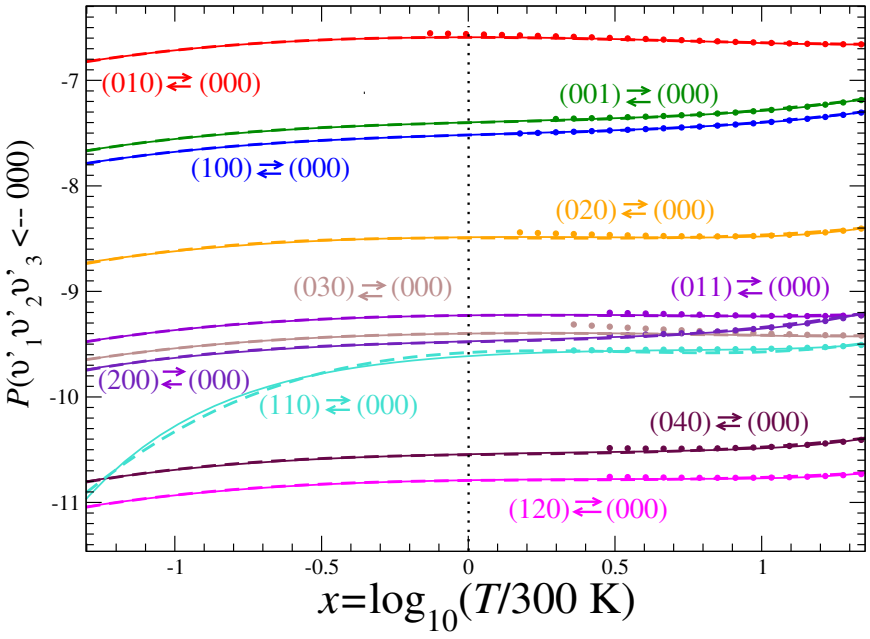

Figure 10. Quality of the fit of Equation (7) for (de-)excitation process of HDO. Numerical and fitted values are displayed by solid and dashed lines according to the color code of Figures 5 and 6, respectively. Circles of the same color refer to the excitation process. For convenience, the vertical dashed line at $x = 0$ gives the coefficient value of a_0 at 300 K, evaluated by the analytical fit as 10^{a_0}, see Equation (7).

3.3. Assessment of Uncertainties

As in many similar theoretical studies, there are two types of uncertainties in the obtained results. One source is due to the approximations made in the theoretical approach, which employs the vibrational frame transformation and neglects the rotational structure and certain non-Born–Oppenheimer couplings in the electron-molecule interaction. The second source is due to the limitation of employed reduced basis sets in the representation of vibrational and electronic motion. We estimate that the major uncertainty of the present results is due to the limited accuracy of the e-HDO scattering calculations. To assess and demonstrate the uncertainty, vibrational excitation cross sections were computed using three different sets (Models 1–3) of electron-scattering parameters. Model 1 is the main set of parameters, discussed above. Model 2 uses a different basis set `DZP`, in Model 3 a smaller complete active space is employed, in which the 1*a*, 2*a* and 3*a* orbitals were kept frozen. Figure 11 compares the cross sections obtained in Models 1–3. Comparing the results of Models 2 and 3 with Model 1, we note that the uncertainty of the bending-mode cross section is estimated to be about 30% at energies 0.2 eV and about 10% at and above 2 eV. Uncertainty of the cross sections for the stretching modes is larger, between 60% and 10% in the same energy interval.

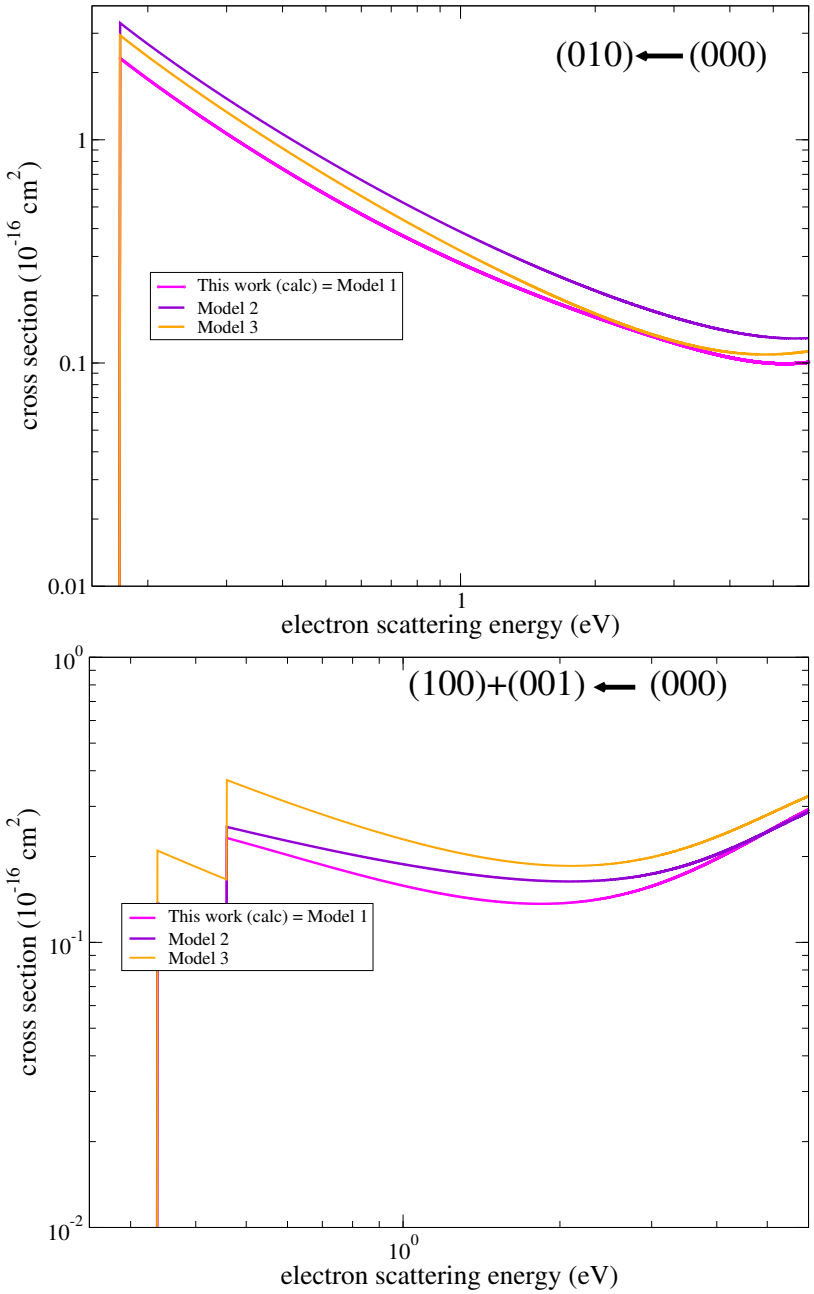

Figure 11. The figure compares the results obtained for the different models, Models 1–3, discussed in the text. It allows us to assess the uncertainty of the obtained theoretical cross sections with respect to the parameters of the calculations. Cross sections for the excitation of the bending mode (the upper panel) and the stretching modes (the lower panel) are shown.

4. Conclusions

Electron-impact excitation of the 16 low-lying vibrational levels of isotopologue HDO of the water molecule was modeled, and the corresponding cross sections were computed using a theoretical approach based on first principles only. The highest considered vibrational level is (130), situated at 6849 cm^{-1} above the ground level. Thermally averaged rate coefficients have been obtained for the 10–10,000 K interval of temperatures. Analytical fits for rate coefficients were provided for convenience of use. The H/D isotopic substitution was found to have a large impact in general, so the rate coefficients for H_2O could not be used reliably for HDO. In order to employ these rate coefficients in modeling non-LTE spectra of HDO in various astrophysical environments, uncertainty estimations were performed. Having both studies on vibrational (de-)excitations of H_2O and HDO,

a model accounting for rotationally resolved vibrational rate coefficients is now being developed and data will be reported in future work. These findings could be incorporated into astrophysical models.

Author Contributions: Conceptualization, M.A.A., A.F. and V.K.; methodology, M.A.A. and V.K.; software, M.A.A.; validation, M.A.A., V.K., A.F., I.F.S. and J.Z.M.; formal analysis, M.A.A., A.F and V.K.; investigation, M.A.A.; resources, M.A.A.; data curation, M.A.A., A.F., I.F.S. and J.Z.M.; writing—original draft preparation, M.A.A.; writing—review and editing, M.A.A., V.K., A.F., I.F.S. and J.Z.M.; visualization, M.A.A.; supervision, M.A.A.; project administration, M.A.A.; funding acquisition, M.A.A., V.K., A.F., I.F.S. and J.Z.M. All authors have read and agreed to the published version of the manuscript.

Funding: This research was funded by the Transatlantic Mobility Program of the Office for Science and Technology of the Embassy of France in the United States, Programme National Physique et Chimie du Milieu Interstellaire (PCMI) of CNRS/INSU, the program "Accueil des chercheurs étranger" of CentraleSupélec and the National Science Foundation, Grant No. PHY-2409570. AF acknowledges support by the French Agence Nationale de la Recherche (ANR-Waterstars), grant number ANR-20-CE31-0011. IFS acknowledges support by the French 'Institut pour Energie, Propulsion et Environnement' (IEPE). JZsM is grateful for financial support from the National Research, Development and Innovation Fund of Hungary, under the FK 19 funding schemes with Project Number FK 132989.

Data Availability Statement: Data are contained within the article.

Conflicts of Interest: The authors declare no conflicts of interest.

Appendix A. Fitting Parameters for the Calculated Rate Coefficients

We provide in the tables below the fitting parameters for the obtained rate coefficients.

Table A1. Parameters a_0, a_1, a_2, and a_3 of the fitting polynomial $P(v' \leftarrow v)$ of Equations (6) and (7) for transitions to the ground vibrational level from the nine lowest vibrational levels of HDO. The second column gives energies $\Delta_{v',v}$ (experimental energies) in Equation (8).

$v_1'v_2'v_3' \leftarrow v_1v_2v_3$	$\Delta_{v_1'v_2'v_3',v_1v_2v_3}$ (K)	a_0	a_1	a_2	a_3
000 ← 010	0.0	−6.59	-4.74×10^{-3}	-8.68×10^{-2}	4.06×10^{-2}
000 ← 100	0.0	−7.52	7.82×10^{-2}	-1.95×10^{-2}	6.13×10^{-2}
000 ← 020	0.0	−8.49	1.52×10^{-3}	-4.71×10^{-2}	7.29×10^{-2}
000 ← 001	0.0	−7.40	6.87×10^{-2}	-1.79×10^{-2}	6.69×10^{-2}
000 ← 030	0.0	−9.40	2.68×10^{-2}	-7.94×10^{-2}	3.55×10^{-2}
000 ← 110	0.0	−9.58	1.47×10^{-1}	-3.72×10^{-1}	2.30×10^{-1}
000 ← 011	0.0	−9.23	2.28×10^{-2}	-7.14×10^{-2}	4.45×10^{-2}
000 ← 200	0.0	−9.48	6.05×10^{-2}	-5.46×10^{-3}	8.16×10^{-2}
000 ← 040	0.0	−10.50	3.78×10^{-2}	-3.46×10^{-2}	6.84×10^{-2}
000 ← 120	0.0	−10.80	2.84×10^{-2}	-5.52×10^{-2}	5.54×10^{-2}
000 ← 021	0.0	−10.10	7.55×10^{-2}	-2.79×10^{-2}	5.47×10^{-2}
000 ← 101	0.0	−9.90	7.30×10^{-2}	-4.94×10^{-2}	3.72×10^{-2}
000 ← 050	0.0	−13.70	6.45×10^{-2}	-1.78×10^{-2}	7.04×10^{-2}
000 ← 210	0.0	−11.8	2.60×10^{-2}	-1.37×10^{-2}	9.12×10^{-2}
000 ← 130	0.0	−12.40	1.09×10^{-2}	-3.84×10^{-2}	7.86×10^{-2}

Table A2. Same as Table A1 for transitions to (010).

$v_1'v_2'v_3' \leftarrow v_1v_2v_3$	$\Delta_{v_1'v_2'v_3',v_1v_2v_3}$ (K)	a_0	a_1	a_2	a_3
010 ← 000	2019.0	−6.56	-2.91×10^{-2}	-1.10×10^{-1}	5.97×10^{-2}
010 ← 100	0.0	−7.40	-5.67×10^{-3}	-8.73×10^{-2}	4.05×10^{-2}
010 ← 020	0.0	−6.33	-2.57×10^{-3}	-8.64×10^{-2}	4.01×10^{-2}
010 ← 001	0.0	−8.47	9.79×10^{-3}	-7.82×10^{-2}	4.31×10^{-2}
010 ← 110	0.0	−7.82	1.70×10^{-1}	-3.38×10^{-1}	2.46×10^{-1}
010 ← 030	0.0	−7.68	7.07×10^{-2}	-2.48×10^{-2}	5.96×10^{-2}
010 ← 011	0.0	−7.43	7.18×10^{-2}	-1.52×10^{-2}	6.76×10^{-2}
010 ← 200	0.0	−9.75	3.28×10^{-2}	-7.19×10^{-2}	3.88×10^{-2}
010 ← 040	0.0	−9.38	2.40×10^{-2}	-8.60×10^{-2}	3.10×10^{-2}
010 ← 120	0.0	−9.08	2.86×10^{-2}	-6.18×10^{-2}	4.95×10^{-2}
010 ← 101	0.0	−9.43	2.17×10^{-2}	-7.89×10^{-2}	3.87×10^{-2}
010 ← 021	0.0	−9.11	2.60×10^{-2}	-6.53×10^{-2}	4.81×10^{-2}
010 ← 050	0.0	−11.50	8.39×10^{-2}	4.22×10^{-2}	1.06×10^{-1}
010 ← 210	0.0	−9.54	6.36×10^{-2}	-1.14×10^{-3}	8.38×10^{-2}
010 ← 130	0.0	−10.10	3.34×10^{-2}	-4.61×10^{-2}	6.07×10^{-2}

Table A3. Same as Table A1 for transitions to (100).

$v_1'v_2'v_3' \leftarrow v_1v_2v_3$	$\Delta_{v_1'v_2'v_3',v_1v_2v_3}$ (K)	a_0	a_1	a_2	a_3
100 ← 000	3919.0	−7.53	1.28×10^{-1}	-9.39×10^{-2}	9.00×10^{-2}
100 ← 010	1899.0	−7.37	-3.03×10^{-2}	-1.11×10^{-1}	6.00×10^{-2}
100 ← 020	0.0	−7.97	-1.50×10^{-1}	-1.11×10^{-1}	6.36×10^{-2}
100 ← 001	0.0	−8.88	-1.83×10^{-2}	-7.66×10^{-2}	5.29×10^{-2}
100 ← 110	0.0	−7.41	1.10×10^{-1}	-4.01×10^{-1}	2.19×10^{-1}
100 ← 030	0.0	−6.60	-8.83×10^{-4}	-8.57×10^{-2}	4.01×10^{-2}
100 ← 011	0.0	−9.34	3.48×10^{-3}	-6.70×10^{-2}	5.56×10^{-2}
100 ← 200	0.0	−7.23	7.97×10^{-2}	-1.82×10^{-2}	6.16×10^{-2}
100 ← 040	0.0	−8.52	-1.68×10^{-2}	-7.02×10^{-2}	6.21×10^{-2}
100 ← 120	0.0	−8.78	3.79×10^{-2}	-4.66×10^{-2}	5.58×10^{-2}
100 ← 101	0.0	−7.72	6.64×10^{-2}	-2.04×10^{-2}	6.59×10^{-2}
100 ← 021	0.0	−7.68	7.01×10^{-2}	-1.68×10^{-2}	6.71×10^{-2}
100 ← 050	0.0	−9.73	2.40×10^{-2}	-8.48×10^{-2}	3.20×10^{-2}
100 ← 210	0.0	−8.80	3.09×10^{-2}	-6.23×10^{-2}	4.80×10^{-2}
100 ← 130	0.0	−10.90	3.15×10^{-2}	-3.96×10^{-2}	6.57×10^{-2}

Table A4. Same as Table A1 for transitions to (020).

$v_1'v_2'v_3' \leftarrow v_1v_2v_3$	$\Delta_{v_1'v_2'v_3',v_1v_2v_3}$ (K)	a_0	a_1	a_2	a_3
020 ← 000	4003.0	−8.45	4.68×10^{-2}	-2.45×10^{-1}	1.75×10^{-1}
020 ← 010	1983.0	−6.29	-3.97×10^{-2}	-9.80×10^{-2}	5.55×10^{-2}
020 ← 100	84.0	−7.93	-2.87×10^{-1}	2.26×10^{-1}	-1.29×10^{-1}
020 ← 001	0.0	−9.00	-2.94×10^{-2}	-1.04×10^{-1}	3.46×10^{-2}
020 ← 110	0.0	−6.38	1.17×10^{-1}	-4.00×10^{-1}	2.17×10^{-1}
020 ← 030	0.0	−6.55	1.22×10^{-3}	-8.55×10^{-2}	3.94×10^{-2}
020 ← 011	0.0	−8.23	1.51×10^{-2}	-7.73×10^{-2}	4.17×10^{-2}
020 ← 200	0.0	−8.79	4.42×10^{-2}	-3.51×10^{-2}	6.36×10^{-2}
020 ← 040	0.0	−7.72	4.65×10^{-2}	-3.62×10^{-2}	6.02×10^{-2}
020 ← 120	0.0	−7.66	5.73×10^{-2}	-2.10×10^{-2}	6.92×10^{-2}
020 ← 101	0.0	−7.70	7.25×10^{-2}	-1.50×10^{-2}	6.74×10^{-2}
020 ← 021	0.0	−7.81	7.60×10^{-2}	-1.13×10^{-2}	6.88×10^{-2}
020 ← 050	0.0	−9.21	2.12×10^{-2}	-8.46×10^{-2}	3.33×10^{-2}
020 ← 210	0.0	−10.80	9.58×10^{-2}	-1.28×10^{-2}	5.91×10^{-2}
020 ← 130	0.0	−8.91	2.92×10^{-2}	-5.94×10^{-2}	5.11×10^{-2}

Table A5. Same as Table A1 for transitions to (001).

$v_1'v_2'v_3' \leftarrow v_1v_2v_3$	$\Delta_{v_1'v_2'v_3',v_1v_2v_3}$ (K)	a_0	a_1	a_2	a_3
001 ← 000	5334.0	−7.38	5.62×10^{-2}	-4.76×10^{-2}	8.40×10^{-2}
001 ← 010	3315.0	−8.43	2.28×10^{-2}	-1.76×10^{-1}	9.42×10^{-2}
001 ← 100	1415.0	−8.85	-4.49×10^{-2}	-1.04×10^{-1}	7.68×10^{-2}
001 ← 020	1332.0	−8.98	-5.37×10^{-2}	-1.06×10^{-1}	4.13×10^{-2}
001 ← 110	0.0	−10.30	-5.07×10^{-2}	-3.57×10^{-1}	3.04×10^{-1}
001 ← 030	0.0	−11.30	1.22×10^{-1}	8.37×10^{-2}	1.09×10^{-1}
001 ← 011	0.0	−6.58	-4.62×10^{-3}	-8.67×10^{-2}	4.07×10^{-2}
001 ← 200	0.0	−9.98	1.89×10^{-2}	-7.90×10^{-2}	3.76×10^{-2}
001 ← 040	0.0	−10.40	3.89×10^{-3}	-8.60×10^{-2}	3.83×10^{-2}
001 ← 120	0.0	−11.70	5.61×10^{-2}	-2.04×10^{-2}	7.31×10^{-2}
001 ← 101	0.0	−7.68	7.22×10^{-2}	-1.80×10^{-2}	6.52×10^{-2}
001 ← 021	0.0	−7.87	6.83×10^{-2}	-2.86×10^{-2}	5.78×10^{-2}
001 ← 050	0.0	−11.90	-3.78×10^{-2}	-5.58×10^{-2}	8.42×10^{-2}
001 ← 210	0.0	−10.40	6.45×10^{-2}	-3.18×10^{-2}	5.72×10^{-2}
001 ← 130	0.0	−11.40	7.66×10^{-2}	-2.23×10^{-2}	5.96×10^{-2}

Table A6. Same as Table A1 for transitions to (110).

$v_1'v_2'v_3' \leftarrow v_1v_2v_3$	$\Delta_{v_1'v_2'v_3',v_1v_2v_3}$ (K)	a_0	a_1	a_2	a_3
110 ← 000	5899.0	−9.62	2.54×10^{-1}	-3.35×10^{-1}	1.55×10^{-1}
110 ← 010	3880.0	−7.81	1.31×10^{-1}	-1.66×10^{-1}	1.31×10^{-1}
110 ← 100	1980.0	−7.42	8.23×10^{-2}	-2.05×10^{-1}	8.87×10^{-2}
110 ← 020	1896.0	−6.39	9.84×10^{-2}	-2.02×10^{-1}	8.34×10^{-2}
110 ← 001	565.0	−10.30	-4.01×10^{-2}	-2.91×10^{-1}	2.50×10^{-1}
110 ← 030	0.0	−7.46	-1.49×10^{-1}	-1.12×10^{-1}	6.22×10^{-2}
110 ← 011	0.0	−8.51	-1.57×10^{-2}	-9.79×10^{-2}	3.51×10^{-2}
110 ← 200	0.0	−9.68	4.65×10^{-2}	-7.19×10^{-2}	3.38×10^{-2}
110 ← 040	0.0	−6.82	2.31×10^{-3}	-8.55×10^{-2}	3.88×10^{-2}
110 ← 120	0.0	−6.23	-3.01×10^{-4}	-8.57×10^{-2}	3.97×10^{-2}
110 ← 101	0.0	−8.34	1.34×10^{-2}	-7.43×10^{-2}	4.50×10^{-2}
110 ← 021	0.0	−8.94	3.21×10^{-2}	-7.44×10^{-2}	3.65×10^{-2}
110 ← 050	0.0	−8.17	5.33×10^{-3}	-6.08×10^{-2}	5.84×10^{-2}
110 ← 210	0.0	−7.60	8.32×10^{-2}	-1.69×10^{-2}	6.10×10^{-2}
110 ← 130	0.0	−7.63	3.81×10^{-2}	-2.79×10^{-2}	7.21×10^{-2}

Table A7. Same as Table A1 for transitions to (030).

$v_1'v_2'v_3' \leftarrow v_1v_2v_3$	$\Delta_{v_1'v_2'v_3',v_1v_2v_3}$ (K)	a_0	a_1	a_2	a_3
030 ← 000	5964.0	−9.29	-4.45×10^{-2}	-1.42×10^{-1}	7.79×10^{-2}
030 ← 010	3945.0	−7.55	-1.49×10^{-1}	9.67×10^{-2}	3.73×10^{-2}
030 ← 100	2046.0	−6.41	-3.39×10^{-1}	1.30×10^{-1}	-6.23×10^{-3}
030 ← 020	1962.0	−6.36	-3.27×10^{-1}	1.24×10^{-1}	-6.26×10^{-3}
030 ← 001	630.0	−11.10	-3.49×10^{-1}	4.98×10^{-1}	-1.59×10^{-2}
030 ← 110	65.0	−7.43	-2.30×10^{-1}	8.37×10^{-2}	-4.92×10^{-2}
030 ← 011	0.0	−9.71	-1.19×10^{-1}	-3.22×10^{-2}	1.24×10^{-1}
030 ← 200	0.0	−7.38	-4.28×10^{-3}	-8.74×10^{-2}	4.00×10^{-2}
030 ← 040	0.0	−6.13	3.15×10^{-4}	-8.58×10^{-2}	3.94×10^{-2}
030 ← 120	0.0	−7.96	-1.80×10^{-2}	-8.68×10^{-2}	4.60×10^{-2}
030 ← 101	0.0	−10.20	7.22×10^{-2}	-5.19×10^{-2}	3.76×10^{-2}
030 ← 021	0.0	−8.23	1.48×10^{-2}	-7.25×10^{-2}	4.60×10^{-2}
030 ← 050	0.0	−7.61	2.58×10^{-2}	-4.73×10^{-2}	6.02×10^{-2}
030 ← 210	0.0	−7.48	7.71×10^{-2}	-1.82×10^{-2}	6.29×10^{-2}
030 ← 130	0.0	−8.24	8.01×10^{-2}	-1.81×10^{-2}	6.14×10^{-2}

Table A8. Same as Table A1 for transitions to (011).

$v_1'v_2'v_3' \leftarrow v_1v_2v_3$	$\Delta_{v_1'v_2'v_3',v_1v_2v_3}$ (K)	a_0	a_1	a_2	a_3
011 ← 000	7323.0	−9.23	1.63×10^{-1}	-2.99×10^{-1}	1.33×10^{-1}
011 ← 010	5303.0	−7.35	-6.01×10^{-2}	4.11×10^{-2}	6.25×10^{-2}
011 ← 100	3404.0	−9.29	1.76×10^{-2}	-2.05×10^{-1}	1.30×10^{-1}
011 ← 020	3320.0	−8.18	1.14×10^{-2}	-1.56×10^{-1}	8.56×10^{-2}
011 ← 001	1988.0	−6.47	-1.74×10^{-1}	-9.82×10^{-4}	3.04×10^{-2}
011 ← 110	1424.0	−8.41	-2.02×10^{-1}	2.70×10^{-2}	5.97×10^{-3}
011 ← 030	1358.0	−9.54	-3.62×10^{-1}	1.67×10^{-2}	1.58×10^{-1}
011 ← 200	0.0	−10.70	-2.80×10^{-2}	-4.06×10^{-2}	8.75×10^{-2}
011 ← 040	0.0	−10.10	1.32×10^{-2}	-7.85×10^{-2}	3.39×10^{-2}
011 ← 120	0.0	−9.84	-1.43×10^{-1}	-4.28×10^{-2}	1.20×10^{-1}
011 ← 101	0.0	−6.84	-3.66×10^{-3}	-8.68×10^{-2}	4.02×10^{-2}
011 ← 021	0.0	−6.42	-1.55×10^{-3}	-8.57×10^{-2}	4.02×10^{-2}
011 ← 050	0.0	−9.77	-8.72×10^{-3}	-8.83×10^{-2}	4.18×10^{-2}
011 ← 210	0.0	−10.20	2.07×10^{-2}	-7.99×10^{-2}	3.60×10^{-2}
011 ← 130	0.0	−11.30	7.89×10^{-2}	-9.20×10^{-3}	7.24×10^{-2}

Table A9. Same as Table A1 for transitions to (200).

$v_1'v_2'v_3' \leftarrow v_1v_2v_3$	$\Delta_{v_1'v_2'v_3',v_1v_2v_3}$ (K)	a_0	a_1	a_2	a_3
200 ← 000	7717.0	−9.35	-2.31×10^{-1}	2.05×10^{-1}	2.61×10^{-2}
200 ← 010	5698.0	−9.77	1.65×10^{-1}	-2.53×10^{-1}	1.05×10^{-1}
200 ← 100	3799.0	−7.18	3.36×10^{-2}	-2.62×10^{-2}	7.41×10^{-2}
200 ← 020	3715.0	−8.76	5.81×10^{-2}	-1.40×10^{-1}	1.19×10^{-1}
200 ← 001	2383.0	−9.95	-1.88×10^{-3}	-9.87×10^{-2}	5.24×10^{-2}
200 ← 110	1818.0	−9.66	3.91×10^{-2}	-1.05×10^{-1}	5.33×10^{-2}
200 ← 030	1753.0	−7.33	-7.90×10^{-2}	-6.55×10^{-2}	4.50×10^{-2}
200 ← 011	395.0	−10.70	-1.74×10^{-1}	5.08×10^{-2}	7.44×10^{-2}
200 ← 040	0.0	−7.73	-1.34×10^{-1}	-1.07×10^{-1}	6.04×10^{-2}
200 ← 120	0.0	−9.39	-7.53×10^{-2}	-8.64×10^{-2}	5.50×10^{-2}
200 ← 101	0.0	−8.41	-1.47×10^{-2}	-8.63×10^{-2}	4.43×10^{-2}
200 ← 021	0.0	−9.04	-2.09×10^{-2}	-7.34×10^{-2}	5.69×10^{-2}
200 ← 050	0.0	−7.12	1.08×10^{-3}	-8.57×10^{-2}	3.93×10^{-2}
200 ← 210	0.0	−6.67	-5.60×10^{-3}	-8.65×10^{-2}	4.11×10^{-2}
200 ← 130	0.0	−8.58	-4.43×10^{-3}	-8.58×10^{-2}	4.14×10^{-2}

Table A10. Same as Table A1 for transitions to (040).

$v_1'v_2'v_3' \leftarrow v_1v_2v_3$	$\Delta_{v_1'v_2'v_3',v_1v_2v_3}$ (K)	a_0	a_1	a_2	a_3
040 ← 000	7798.0	−10.40	-9.53×10^{-2}	-3.15×10^{-2}	8.97×10^{-2}
040 ← 010	5779.0	−9.35	8.33×10^{-2}	-2.20×10^{-1}	8.62×10^{-2}
040 ← 100	3879.0	−8.44	-2.06×10^{-2}	-2.58×10^{-1}	1.68×10^{-1}
040 ← 020	3796.0	−7.62	-9.95×10^{-2}	2.05×10^{-2}	5.92×10^{-2}
040 ← 001	2464.0	−10.30	-1.21×10^{-1}	-4.51×10^{-2}	4.22×10^{-2}
040 ← 110	1899.0	−6.73	-1.42×10^{-1}	-1.12×10^{-2}	2.91×10^{-2}
040 ← 030	1834.0	−6.02	-1.86×10^{-1}	1.79×10^{-2}	2.26×10^{-2}
040 ← 011	476.0	−9.97	-2.93×10^{-1}	2.44×10^{-1}	-8.37×10^{-2}
040 ← 200	81.0	−7.65	-3.84×10^{-1}	5.15×10^{-1}	-2.94×10^{-1}
040 ← 120	0.0	−7.67	-1.33×10^{-1}	-1.08×10^{-1}	5.73×10^{-2}
040 ← 101	0.0	−9.82	-1.20×10^{-1}	-7.77×10^{-2}	9.36×10^{-2}
040 ← 021	0.0	−8.55	-2.07×10^{-2}	-9.83×10^{-2}	3.68×10^{-2}
040 ← 050	0.0	−5.96	2.88×10^{-3}	-8.54×10^{-2}	3.89×10^{-2}
040 ← 210	0.0	−7.25	3.37×10^{-3}	-8.49×10^{-2}	3.89×10^{-2}
040 ← 130	0.0	−9.24	-4.27×10^{-2}	-5.06×10^{-2}	8.34×10^{-2}

Table A11. Same as Table A1 for transitions to (120).

$v_1'v_2'v_3' \leftarrow v_1v_2v_3$	$\Delta_{v_1'v_2'v_3',v_1v_2v_3}$ (K)	a_0	a_1	a_2	a_3
120 ← 000	7922.0	−10.80	6.96×10^{-2}	-1.87×10^{-1}	1.13×10^{-1}
120 ← 010	5903.0	−9.04	8.26×10^{-2}	-2.27×10^{-1}	1.24×10^{-1}
120 ← 100	4003.0	-8.73	-9.34×10^{-3}	-7.01×10^{-2}	7.80×10^{-2}
120 ← 020	3919.0	−7.56	-6.47×10^{-2}	-1.50×10^{-2}	9.16×10^{-2}
120 ← 001	2588.0	−11.70	-8.99×10^{-3}	-1.11×10^{-1}	1.41×10^{-1}
120 ← 110	2023.0	−6.14	-1.56×10^{-1}	-6.57×10^{-3}	2.98×10^{-2}
120 ← 030	1958.0	−7.84	-2.08×10^{-1}	-3.95×10^{-3}	4.28×10^{-2}
120 ← 011	599.0	−9.66	-4.69×10^{-1}	1.24×10^{-1}	1.05×10^{-1}
120 ← 200	205.0	−9.32	-2.67×10^{-1}	1.66×10^{-1}	-5.33×10^{-2}
120 ← 040	124.0	−7.61	-3.09×10^{-1}	1.81×10^{-1}	-8.37×10^{-2}
120 ← 101	0.0	−8.53	-2.02×10^{-2}	-1.00×10^{-1}	3.46×10^{-2}
120 ← 021	0.0	−8.84	1.20×10^{-3}	-8.83×10^{-2}	3.64×10^{-2}
120 ← 050	0.0	−7.57	9.46×10^{-3}	-8.38×10^{-2}	3.75×10^{-2}
120 ← 210	0.0	−7.26	-1.94×10^{-3}	-8.69×10^{-2}	3.94×10^{-2}
120 ← 130	0.0	−6.12	8.98×10^{-4}	-8.53×10^{-2}	3.95×10^{-2}

Table A12. Same as Table A1 for transitions to (101).

$v_1'v_2'v_3' \leftarrow v_1v_2v_3$	$\Delta_{v_1'v_2'v_3',v_1v_2v_3}$ (K)	a_0	a_1	a_2	a_3
101 ← 000	9230.0	−9.84	-1.01×10^{-1}	1.61×10^{-1}	-4.73×10^{-2}
101 ← 010	7211.0	−9.47	2.39×10^{-1}	-3.53×10^{-1}	1.37×10^{-1}
101 ← 100	5312.0	−7.73	1.14×10^{-1}	-9.55×10^{-2}	9.54×10^{-2}
101 ← 020	5228.0	−7.66	2.04×10^{-2}	-1.11×10^{-2}	7.45×10^{-2}
101 ← 001	3896.0	−7.67	9.01×10^{-2}	-8.64×10^{-2}	9.79×10^{-2}
101 ← 110	3331.0	−8.34	8.75×10^{-2}	-2.17×10^{-1}	1.08×10^{-1}
101 ← 030	3266.0	−10.20	5.44×10^{-2}	-5.29×10^{-2}	3.84×10^{-2}
101 ← 011	1908.0	−6.80	-5.36×10^{-2}	-8.89×10^{-2}	5.31×10^{-2}
101 ← 200	1513.0	−8.42	2.85×10^{-2}	-1.58×10^{-1}	7.71×10^{-2}
101 ← 040	1432.0	−9.82	-3.42×10^{-2}	-3.10×10^{-1}	2.17×10^{-1}
101 ← 120	1308.0	−8.48	-1.00×10^{-1}	-5.44×10^{-2}	2.67×10^{-2}
101 ← 021	0.0	−7.58	-1.76×10^{-1}	-1.18×10^{-1}	6.57×10^{-2}
101 ← 050	0.0	−9.72	-9.64×10^{-3}	-8.63×10^{-2}	3.76×10^{-2}
101 ← 210	0.0	−10.30	-2.39×10^{-1}	-9.16×10^{-3}	1.70×10^{-1}
101 ← 130	0.0	−9.61	-1.31×10^{-1}	-6.50×10^{-2}	9.83×10^{-2}

Table A13. Same as Table A1 for transitions to (021).

$v_1'v_2'v_3' \leftarrow v_1v_2v_3$	$\Delta_{v_1'v_2'v_3',v_1v_2v_3}$ (K)	a_0	a_1	a_2	a_3
021 ← 000	9283.0	−9.88	-3.79×10^{-1}	3.64×10^{-1}	-7.03×10^{-2}
021 ← 010	7264.0	−9.02	-2.36×10^{-3}	-1.73×10^{-1}	1.07×10^{-1}
021 ← 100	5364.0	−7.53	-1.91×10^{-1}	1.22×10^{-1}	4.36×10^{-2}
021 ← 020	5280.0	−7.66	-1.98×10^{-1}	1.50×10^{-1}	3.59×10^{-2}
021 ← 001	3949.0	−7.74	-1.49×10^{-1}	8.54×10^{-2}	3.92×10^{-2}
021 ← 110	3384.0	−8.81	-1.54×10^{-1}	5.43×10^{-3}	2.97×10^{-2}
021 ← 030	3318.0	−8.08	-1.74×10^{-1}	-4.00×10^{-2}	6.75×10^{-2}
021 ← 011	1960.0	−6.24	-3.24×10^{-1}	1.17×10^{-1}	-2.69×10^{-3}
021 ← 200	1565.0	−8.84	-3.78×10^{-1}	1.36×10^{-1}	1.98×10^{-2}
021 ← 040	1485.0	−8.35	-3.96×10^{-1}	1.66×10^{-1}	-2.91×10^{-2}
021 ← 120	1361.0	−8.66	-3.65×10^{-1}	1.84×10^{-1}	-3.57×10^{-2}
021 ← 101	52.0	−7.52	-3.40×10^{-1}	2.83×10^{-1}	-1.63×10^{-1}
021 ← 050	0.0	−9.32	7.34×10^{-3}	-8.42×10^{-2}	3.38×10^{-2}
021 ← 210	0.0	−10.10	-1.62×10^{-1}	2.11×10^{-2}	1.68×10^{-1}
021 ← 130	0.0	−9.99	-1.10×10^{-1}	-5.21×10^{-2}	1.01×10^{-1}

Table A14. Same as Table A1 for transitions to (021).

$v_1'v_2'v_3' \leftarrow v_1v_2v_3$	$\Delta_{v_1'v_2'v_3',v_1v_2v_3}$ (K)	a_0	a_1	a_2	a_3
050 ← 000	9626.0	−13.50	-2.82×10^{-1}	2.45×10^{-1}	-8.39×10^{-3}
050 ← 010	7607.0	−11.10	-8.69×10^{-1}	9.51×10^{-1}	-1.87×10^{-1}
050 ← 100	5707.0	−9.69	6.52×10^{-2}	-2.09×10^{-1}	8.55×10^{-2}
050 ← 020	5623.0	−9.17	6.66×10^{-2}	-2.13×10^{-1}	8.89×10^{-2}
050 ← 001	4292.0	−11.80	-2.64×10^{-2}	-3.28×10^{-1}	2.36×10^{-1}
050 ← 110	3727.0	−8.06	-1.25×10^{-1}	-6.63×10^{-2}	8.97×10^{-2}
050 ← 030	3662.0	−7.54	-6.98×10^{-2}	-4.73×10^{-2}	8.08×10^{-2}
050 ← 011	2303.0	−9.68	-1.41×10^{-1}	-4.94×10^{-2}	4.96×10^{-2}
050 ← 200	1909.0	−7.02	-1.71×10^{-1}	7.77×10^{-3}	2.49×10^{-2}
050 ← 040	1828.0	−5.86	-1.67×10^{-1}	8.27×10^{-3}	2.38×10^{-2}
050 ← 120	1704.0	−7.47	-1.63×10^{-1}	2.50×10^{-2}	1.45×10^{-2}
050 ← 101	396.0	−9.59	-3.17×10^{-1}	2.46×10^{-1}	-8.56×10^{-2}
050 ← 021	343.0	−9.23	-2.50×10^{-1}	2.13×10^{-1}	-8.14×10^{-2}
050 ← 210	0.0	−7.88	-1.37×10^{-1}	-1.10×10^{-1}	5.80×10^{-2}
050 ← 130	0.0	−8.09	-1.13×10^{-1}	-1.08×10^{-1}	5.11×10^{-2}

Table A15. Same as Table A1 for transitions to (210).

$v_1'v_2'v_3' \leftarrow v_1v_2v_3$	$\Delta_{v_1'v_2'v_3',v_1v_2v_3}$ (K)	a_0	a_1	a_2	a_3
210 ← 000	9707.0	−11.40	-8.75×10^{-1}	7.08×10^{-1}	-1.09×10^{-1}
210 ← 010	7688.0	−9.39	-2.84×10^{-1}	2.59×10^{-1}	1.31×10^{-2}
210 ← 100	5789.0	−8.76	6.86×10^{-2}	-2.11×10^{-1}	1.17×10^{-1}
210 ← 020	5705.0	−10.70	-2.56×10^{-2}	6.10×10^{-2}	3.88×10^{-2}
210 ← 001	4373.0	−10.40	6.02×10^{-3}	-4.26×10^{-2}	7.32×10^{-2}
210 ← 110	3808.0	−7.55	1.50×10^{-3}	1.15×10^{-2}	6.08×10^{-2}
210 ← 030	3743.0	−7.41	-2.19×10^{-2}	3.35×10^{-3}	7.07×10^{-2}
210 ← 011	2385.0	−10.10	-1.17×10^{-1}	-9.40×10^{-3}	2.53×10^{-2}
210 ← 200	1990.0	−6.56	-1.79×10^{-1}	1.02×10^{-3}	3.07×10^{-2}
210 ← 040	1909.0	−7.15	-1.70×10^{-1}	1.17×10^{-2}	2.29×10^{-2}
210 ← 120	1785.0	−7.16	-1.62×10^{-1}	-5.08×10^{-3}	2.90×10^{-2}
210 ← 101	477.0	−10.20	-4.19×10^{-1}	1.95×10^{-2}	2.04×10^{-1}
210 ← 021	424.0	−9.97	-4.69×10^{-1}	2.04×10^{-1}	1.40×10^{-1}
210 ← 050	81.0	−7.84	-2.68×10^{-1}	2.08×10^{-1}	-1.22×10^{-1}
210 ← 130	0.0	−7.76	-1.10×10^{-1}	-9.94×10^{-2}	5.51×10^{-2}

Table A16. Same as Table A1 for transitions to (130).

$v_1'v_2'v_3' \leftarrow v_1v_2v_3$	$\Delta_{v_1'v_2'v_3',v_1v_2v_3}$ (K)	a_0	a_1	a_2	a_3
130 ← 000	9854.0	−12.20	-4.74×10^{-1}	2.44×10^{-1}	2.25×10^{-2}
130 ← 010	7835.0	−10.00	-2.75×10^{-2}	-1.05×10^{-1}	9.97×10^{-2}
130 ← 100	5935.0	−10.80	-1.08×10^{-1}	-3.92×10^{-2}	9.31×10^{-2}
130 ← 020	5851.0	−8.83	1.80×10^{-2}	-1.83×10^{-1}	1.17×10^{-1}
130 ← 001	4520.0	−11.30	-6.57×10^{-2}	4.13×10^{-2}	5.19×10^{-2}
130 ← 110	3955.0	−7.54	-5.39×10^{-2}	-7.11×10^{-2}	1.16×10^{-1}
130 ← 030	3890.0	−8.13	-9.82×10^{-2}	7.36×10^{-2}	4.69×10^{-2}
130 ← 011	2531.0	−11.20	-6.30×10^{-2}	-1.97×10^{-2}	1.12×10^{-1}
130 ← 200	2137.0	−8.44	-2.38×10^{-1}	3.64×10^{-2}	2.42×10^{-2}
130 ← 040	2056.0	−9.08	-2.68×10^{-1}	-6.19×10^{-3}	1.12×10^{-1}
130 ← 120	1932.0	−5.98	-2.39×10^{-1}	5.88×10^{-2}	1.16×10^{-2}
130 ← 101	624.0	−9.47	-3.87×10^{-1}	6.80×10^{-2}	8.65×10^{-2}
130 ← 021	571.0	−9.80	-4.89×10^{-1}	2.15×10^{-1}	3.94×10^{-2}
130 ← 050	228.0	−7.97	-4.10×10^{-1}	2.55×10^{-1}	-9.86×10^{-2}
130 ← 210	147.0	−7.66	-3.84×10^{-1}	3.20×10^{-1}	-1.42×10^{-1}

References

1. van Dishoeck, E.F.; Kristensen, L.E.; Mottram, J.C.; Benz, A.O.; Bergin, E.A.; Caselli, P.; Herpin, F.; Hogerheijde, M.R.; Johnstone, D.; Liseau, R.; et al. Water in star-forming regions: Physics and chemistry from clouds to disks as probed by Herschel spectroscopy. *Astron. Astrophys.* **2021**, *648*, A24. . [CrossRef]
2. Tobin, J.J.; van't Hoff, M.L.R.; Leemker, M.; van Dishoeck, E.F.; Paneque-Carreño, T.; Furuya, K.; Harsono, D.; Persson, M.V.; Cleeves, L.I.; Sheehan, P.D.; et al. Deuterium-enriched water ties planet-forming disks to comets and protostars. *Nature* **2023**, *615*, 227–230. [CrossRef]

3. Mahieux, A.; Viscardy, S.; Yelle, R.V.; Karyu, H.; Chamberlain, S.; Robert, S.; Piccialli, A.; Trompet, L.; Erwin, J.T.; Ubukata, S.; et al. Unexpected increase of the deuterium to hydrogen ratio in the Venus mesosphere. *Proc. Natl. Acad. Sci. USA* **2024**, *121*, e2401638121. [CrossRef] [PubMed]
4. Tennyson, J.; Yurchenko, S.N.; Zhang, J.; Bowesman, C.A.; Brady, R.P.; Buldyreva, J.; Chubb, K.L.; Gamache, R.R.; Gorman, M.N.; Guest, E.R.; et al. The 2024 release of the ExoMol database: Molecular line lists for exoplanet and other hot atmospheres. *J. Quant. Spectrosc. Radiat. Transfer* **2024**, *326*, 109083. [CrossRef]
5. Voronin, B.A.; Tennyson, J.; Tolchenov, R.N.; Lugovskoy, A.A.; Yurchenko, S.N. A high accuracy computed line list for the HDO molecule. *Mon. Not. R. Astron. Soc.* **2010**, *402*, 492–496. [CrossRef]
6. Villanueva, G.L.; Mumma, M.J.; Bonev, B.P.; Novak, R.E.; Barber, R.J.; Disanti, M.A. Water in planetary and cometary atmospheres: H_2O/HDO transmittance and fluorescence models. *J. Quant. Spectrosc. Radiat. Transfer* **2012**, *113*, 202–220. [CrossRef]
7. García Muñoz, A.; Asensio Ramos, A.; Faure, A. NLTE modelling of water-rich exoplanet atmospheres. Cooling and heating rates. *Icarus* **2024**, *415*, 116080. [CrossRef]
8. Faure, A.; Lique, F.; Loreau, J. The Effect of H_2O and Electron Collisions on Rotational Populations of Cometary CO. In *European Conference on Laboratory Astrophysics ECLA2020*; The Interplay of Dust; Springer: Cham, Switzerland, 2023; pp. 281–286. [CrossRef]
9. Faure, A.; Żółtowski, M.; Wiesenfeld, L.; Lique, F.; Bergeat, A. The rotational excitation of the water isotopologues by molecular hydrogen. *Mon. Not. R. Astron. Soc.* **2024**, *527*, 3087–3093. [CrossRef]
10. Faure, A.; Gorfinkiel, J.D.; Tennyson, J. Electron-impact rotational excitation of water. *Mon. Not. R. Astron. Soc.* **2004**, *347*, 323–333. [CrossRef]
11. García-Vázquez, R.M.; Bergeat, A.; Denis-Alpizar, O.; Faure, A.; Stoecklin, T.; Morales, S.B. Scattering resonances in the rotational excitation of HDO by Ne and normal-H_2: Theory and experiment. *Faraday Discuss.* **2024**, *251*, 205–224. [CrossRef]
12. Ayouz, M.; Faure, A.; Kokoouline, V. Theoretical study of the electron-induced vibrational excitation of H_2O. *Astron. Astrophys.* **2024**, *687*, A3. [CrossRef]
13. Song, M.Y.; Cho, H.; Karwasz, G.P.; Kokoouline, V.; Nakamura, Y.; Tennyson, J.; Faure, A.; Mason, N.J.; Itikawa, Y. Cross Sections for Electron Collisions with H_2O. *J. Phys. Chem. Ref. Data* **2021**, *50*, 023103. [CrossRef]
14. Werner, H.J.; Knowles, P.J.; Knizia, G.; Manby, F.R.; Schütz, M. Molpro: A general-purpose quantum chemistry program package. *WIREs Comput. Mol. Sci.* **2012**, *2*, 242–253. [CrossRef]
15. Tennyson, J.; Brown, D.B.; Munro, J.J.; Rozum, I.; Varambhia, H.N.; Vinci, N. Quantemol-N: An expert system for performing electron molecule collision calculations using the R-matrix method. *J. Phys. Conf. Ser.* **2007**, *86*, 012001. [CrossRef]
16. Ayouz, M.; Faure, A.; Tennyson, J.; Tudorovskaya, M.; Kokoouline, V. Cross sections and rate coefficients for vibrational excitation of H_2O by electron impact. *Atoms* **2021**, *9*, 62. [CrossRef]
17. Shimanouchi, T. Tables of Molecular Vibrational Frequencies: Part 6. *J. Phys. Chem. Ref. Data* **1973**, *2*, 121–162. [CrossRef]
18. Császár, A.G.; Czakó, G.; Furtenbacher, T.; Tennyson, J.; Szalay, V.; Shirin, S.V.; Zobov, N.F.; Polyansky, O.L. On equilibrium structures of the water molecule. *J. Chem. Phys.* **2005**, *122*, 214305. [CrossRef]
19. Tennyson, J. Electron–molecule collision calculations using the R-matrix method. *Phys. Rep.* **2010**, *491*, 29–76. [CrossRef]
20. Carr, J.; Galiatsatos, P.; Gorfinkiel, J.; Harvey, A.; Lysaght, M.; Madden, D.; Mašín, Z.; Plummer, M.; Tennyson, J.; Varambhia, H. UKRmol: A low-energy electron- and positron-molecule scattering suite. *Euro. Phys. J. D* **2012**, *66*, 58. [CrossRef]
21. Kokoouline, V.; Dulieu, O.; Kosloff, R.; Masnou-Seeuws, F. Mapped Fourier methods for long-range molecules: Application to perturbations in the Rb_2 (0_u^+) photoassociation spectrum. *J. Chem. Phys.* **1999**, *110*, 9865. [CrossRef]
22. Mizus, I.I.; Kyuberis, A.A.; Zobov, N.F.; Makhnev, V.Y.; Polyansky, O.L.; Tennyson, J. High-accuracy water potential energy surface for the calculation of infrared spectra. *Philos. Trans. R. Soc. A* **2018**, *376*. [CrossRef] [PubMed]
23. Tennyson, J.; Bernath, P.F.; Brown, L.R.; Campargue, A.; CsÃ¡szÃ¡r, A.G.; Daumont, L.; Gamache, R.R.; Hodges, J.T.; Naumenko, O.V.; Polyansky, O.L.; et al. IUPAC critical evaluation of the rotationalâ€“vibrational spectra of water vapor. Part II: Energy levels and transition wavenumbers for $HD^{16}O$, $HD^{17}O$, and $HD^{18}O$. *J. Quant. Spectrosc. Radiat. Transfer* **2010**, *111*, 2160–2184. . [CrossRef]
24. Zobov, N.F.; Koshelev, M.A.; Makarov, D.S.; Makhnev, V.Y.; Boyarkin, O.V.; Tyuterev, V.G.; Tennyson, J.; Polyansky, O.L. A global line list for HDO between 0 and 35000 cm^{-1} constructed using multiphoton spectra. *J. Quant. Spectrosc. Radiat. Transfer* **2021**, *271*, 107694. [CrossRef]
25. Sironneau, V.T.; Hodges, J.T. Line shapes, positions and intensities of water transitions near 1.28μm. *J. Quant. Spectrosc. Radiat. Transfer* **2015**, *152*, 1–15. [CrossRef]
26. Khakoo, M.A.; Muse, J.; Campbell, C.; Lopes, M.C.A.; Silva, H.; Winstead, C.; McKoy, V. Low energy electron scattering from polyatomic targets. *J. Phys. Conf. Ser.* **2009**, *194*, 012027. [CrossRef]
27. El-Zein, A.A.A.; Brunger, M.J.; Newell, W.R. Excitation of vibrational quanta in water by electron impact. *J. Phys. B At. Mol. Opt. Phys.* **2000**, *33*, 5033. [CrossRef]
28. Shyn, T.W.; Cho, S.Y.; Cravens, T.E. Vibrational-excitation cross sections of water molecules by electron impact. *Phys. Rev. A* **1988**, *38*, 678–682. [CrossRef]

29. Seng, G.; Linder, F. Vibrational excitation of polar molecules by electron impact. II. Direct and resonant excitation in H_2O. *J. Phys. B At. Mol. Phys.* **1976**, *9*, 2539. [CrossRef]
30. Nishimura, T.; Gianturco, F.A. Vibrational excitation of water by low-energy electron scattering: Calculations and experiments. *Europhys. Lett.* **2004**, *65*, 179–185. [CrossRef]
31. CurÃk, R.; CÃ¡rsky, P. Vibrationally inelastic electron scattering on polyatomic molecules by the discrete momentum representation (DMR) method. *J. Phys. B At. Mol. Opt. Phys.* **2003**, *36*, 2165. [CrossRef]
32. Itikawa, Y.; Mason, N. Rotational excitation of molecules by electron collisions. *Phys. Rep.* **2005**, *414*, 1. [CrossRef]
33. Yousfi, M.; Benabdessadok, M.D. Boltzmann equation analysis of electron−molecule collision cross sections in water vapor and ammonia. *J. Appl. Phys.* **1996**, *80*, 6619–6630. [CrossRef]
34. Ayouz, M.A.; Buch, A. Theoretical Study of the Dissociative Recombination and Vibrational (De-)Excitation of $HCNH^+$ and Its Isomers by Electron Impact. *Atoms* **2024**, *12*, 64. [CrossRef]